A dynamic repertoire of wound closure strategies precedes whole-body regeneration

Allison P. Kann and Mansi Srivastava

Department of Organismic and Evolutionary Biology, Museum of Comparative Zoology,
Harvard University, Cambridge, MA 02138

Corresponding Author Emails: allisonkann@fas.harvard.edu, mansi@oeb.harvard.edu

KEYWORDS

Regeneration, wound healing, wound closure, morphogenesis, acoels, epithelium

ABSTRACT

Wound closure is an essential aspect of successful regeneration, often acting as the first morphogenetic event that precedes downstream cellular events. Despite heavy investment in studying whole-body regeneration in many invertebrate systems, the steps by which these organisms heal their wounds remain understudied. Here, we investigate the cellular mechanisms of wound healing in the acoel *Hofstenia miamia*, an invertebrate worm capable of whole-body regeneration. *H. miamia* have two distinct epithelial layers, an outer epidermis and the epithelial lining of their pharynx. By labeling regenerating fragments with an actin dye, we found that *H. miamia* use distinct mechanisms of epithelial wound repair across different injury contexts. In transverse wounds that don't injure the pharyngeal epithelium, the epidermis closes by gradual radial constriction. In contrast, injuries that damage both the epidermis and the pharyngeal epithelium show the formation of long, actin-rich protrusions that cross the wound gap and form heterotypic bridges prior to re-epithelialization. Muscle contraction is required for the formation of heterotypic bridges - when animals are anesthetized and immobile, they are unable to form these cellular bridges, and epidermal cells cannot migrate independently. Global actomyosin contractility also plays a role in repair mechanisms, and pharmacological perturbation of contractility shifts the dynamics of wound closure after amputation. In the presence of blebbistatin, heterotypic bridge formation is inhibited but

homotypic re-epithelialization is accelerated through increased cell crawling. Together, this work identifies mechanisms by which epithelial layers close large wounds *in vivo*, identifying novel heterotypic cellular bridges in wound closure and demonstrating the conservation of actin-mediated processes in an early-diverging phylum.

INTRODUCTION

The ability of animals to regenerate varies substantially across phyla, ranging from more limited, tissue-specific or structural regeneration to extreme cases of whole-body regeneration (WBR), where any missing cell or tissue type can be replaced after amputation[1,2]. Highly regenerative animals undergoing WBR face unique healing challenges and must be able to scarlessly repair virtually any injury prior to downstream regeneration. Most mechanistic studies of wound closure have focused on relatively simple injuries (i.e. damaging only the epidermis) in animals that are not capable of substantial regeneration, generating foundational knowledge about cellular behaviors but lacking a strong connection to downstream regeneration[3–8]. The work on wound closure in regenerative animals has primarily focused on either the formation and function of the 'wound epidermis', a specialized epidermis that covers the injury site and acts as an organizing center to induce downstream regeneration[9–12], or large-scale transcriptional atlases detailing the molecular wound response[13–18]. Some studies have demonstrated the presence of conserved cellular mechanisms in regenerative animals[19–25], but it remains ambiguous how much flexibility exists in closure strategies prior to regeneration. Specifically, it is unclear whether highly regenerative animals employ a uniform healing process regardless of injury context (i.e. major vs. minor wounds, varying geometries and tissue organizations) or if they have a range of mechanisms that can be tailored to different injury conditions.

Previous work has shown the presence of shared mechanisms of wound repair across the metazoan tree of life, including in early-branching lineages such as cnidarians[14,16,19,20], and in protostomes[3,4,21,25–27] and deuterostomes[15,18,28–30]. This suggests a deep conservation of cellular behaviors, evolving prior to the emergence of bilateral symmetry. A fundamental aspect of wound closure and subsequent healing is the process of re-epithelialization, in which a damaged epithelial layer undergoes cellular and morphological changes to re-establish an intact tissue[6]. Wound closure through cell crawling is facilitated through the formation of actin-based membrane protrusions (such as lamellipodia or filopodia) in cells at the periphery of a wound that drive migration into the gap[7,31,32]. Actomyosin contractility is essential in this crawling mechanism for both retraction at the rear of migrating cells and the formation of tension between adhesion points[19,33,34]. Purse string closure is similarly driven by contractility; cells around the wound form a supracellular cable, contracting and bringing the edges of

61 cells inwards to pinch off the gap[31,35,36]. These mechanisms are not mutually exclusive and often work in
62 tandem, bringing the edges of epithelial cells together across the open wound and restoring tissue
63 integrity through the reestablishment of cell junctions[7].

64 Studies both *in vivo* and *in vitro* have revealed that the mechanisms of re-epithelialization vary
65 substantially between wounding conditions, with factors such as wound size, geometry, tissue type,
66 extracellular matrix composition, and life stage of the animal all influencing the mechanism of closure[6,7,
67 19,23,26,4133,38–41]. Large injuries typically involve damage to the underlying extracellular matrix, leading to
68 either wound closure through the formation of actomyosin purse strings, which do not require an intact
69 substrate, and/or the deposition of a transient matrix that provides a substrate for epithelial cell
70 crawling[19,22,24,37,42]. These large injuries also require coordination between layers of cells, often relying on
71 contraction of mesenchymal cells underneath the epithelium to drive closure[29,43,44]. Despite evidence of
72 variable cellular behaviors across wound conditions, most *in vivo* studies have focused on factors that
73 determine whether wounds close or not, rather than the flexibility of large-scale closure strategies within
74 the same system. This is likely due to a few factors. First and foremost, traditional model organisms that
75 have extensive genetic and imaging tools (e.g. *D. melanogaster, M. musculus*) have distinct physiological
76 considerations. Not only are these species incapable of whole-body regeneration, restricting the types of
77 injuries the animal can recover from, but they possess circulatory and immune systems that complicate
78 and contribute to the healing process[44,45]. Second, visualizing wound closure in a quantifiable and
79 reproducible manner typically requires live imaging, which is more feasible to set up for minor wounds
80 (such as a scratch assay, as used in *C. hemisphaerica*[19]) than for large injuries. We therefore have a
81 detailed understanding of some cellular decision-making, like switching between cell crawling and purse
82 string formation depending on substrate[3,19,35,40,46], but less is understood about whether animals utilize the
83 same toolkit of closure strategies across extreme amputations. Studying these cellular processes in
84 nontraditional animals offers a new approach to understanding fundamental aspects of biology,
85 capitalizing on their regenerative properties to ask questions that are infeasible in other species.

86 *Hofstenia miamia* is a marine invertebrate worm belonging to the enigmatic and understudied
87 phylum Xenacoelomorpha, which likely represents an early-diverging animal lineage that is a sister group
88 to all other bilaterians (Fig. 1A-B)[47–49]. *H. miamia* has emerged as a new model system, largely studied for

its ability to undergo whole-body regeneration. Like other animals capable of WBR, such as platyhelminthes, *H. miamia* rely on a population of adult pluripotent stem cells to drive regeneration [50,51]. However, even in conditions that block regeneration (e.g. functional knockdown of required genes or irradiation of proliferative cells[47,50]), damaged fragments are still able to visibly close their wounds – suggesting that healing and regeneration are distinct processes. In addition to their remarkable regenerative ability, *H. miamia* possess a 'tube within a tube' anatomy, with an outer epidermis and a centrally located pharynx lined with an epithelium[52]. This dual-epithelial organization prompts both questions of how complex injuries can heal and how tissues maintain their identity during repair and regeneration.

In this study, we investigate the healing capacity of *H. miamia*, examining whether wound repair mechanisms shift in response to different injury conditions. In relatively simple injuries (e.g. transverse amputations that only damage one epithelial layer, scratch wounds), animals rely on conserved mechanisms of epithelial contraction and migration. In more complex wounds (e.g. asymmetric sagittal wounds and other amputations that damage both epithelial layers), *H. miamia* form novel heterotypic bridges between epithelial layers prior to homotypic re-epithelialization. These bridges are dependent on both global actomyosin tension and contractility generated by neighboring muscle, but the regenerating fragments can modify their repair strategies in the face of mechanical perturbation. *H. miamia* therefore possess an adaptable toolkit of wound closure mechanisms, with flexible strategies to ensure successful repair and downstream regeneration regardless of injury type.

108 **RESULTS**

109 ***Hofstenia miamia* have two distinct, atypical epithelial tissues**

110 The acoel *Hofstenia miamia* can recover from virtually any injury throughout its lifespan, scarlessly
111 healing wounds and rebuilding lost tissues[47,48]. Despite wound closure being an essential prerequisite to
112 this extensive regeneration, the mechanisms of wound closure have not yet been studied in *H. miamia*.
113 To fully understand the dynamics of re-epithelization, we first needed to characterize the epithelial layers
114 of *H. miamia*.

115 *H. miamia* have two distinct epithelial tissues: (1) an outer epidermis that covers the whole
116 animal, and (2) the inner lining of the pharynx, a tube-shaped organ that extends ~1/2 down the anterior-
117 posterior axis (Figure 1C). Although the dynamics of these cells have not yet been studied, previous
118 transgenic labeling has revealed their cellular morphologies[52]. This transgenic labeling (using *EpiA:RFP*
119 animals[52]) enables the visualization of detailed cell morphologies (Figure 1D), but the mosaicism prevents
120 consistent imaging across animals. We found that the cytoskeletal dye SiR-actin robustly labels both
121 layers of epithelial cells in fixed animals and can therefore be used to visualize entire tissues instead of
122 individual cells (Figure 1E-F). The apical side of *H. miamia* epithelial cells resemble epithelia in other
123 systems[53], with the cells organized in a polygonal pattern on the surface of the animal (Figure 1E). As
124 previously reported, the basal side of both epidermal and pharyngeal epithelial cells form cytoplasmic
125 protrusions that extend into the body of the worm (Figure 1F-H). The protrusions are irregularly spaced
126 and heterogeneous in number between cells but extend approximately 10-25μm in length, with the
127 epidermal protrusions being slightly (but significantly) longer than those in the pharyngeal epithelium
128 (Figure 1G). The basal protrusions in both cell types end in close proximity to underlying muscle (Figure
129 1H), but it is unclear whether cell-cell junctions form at the tips of these projections or whether they
130 adhere to an atypical basement membrane.

131 The unique morphology and organization of these tissues raise questions of how epithelial cells
132 mobilize to close wounds upon amputation and facilitate downstream regeneration. Even though *H.*
133 *miamia* can recover from virtually any injury configuration, not all injuries require the same cellular
134 response. Notably, the internal localization of the pharynx means that some amputations will damage
135 both epithelial layers, adding another layer of complexity to the re-epithelialization process. We therefore

136 sought to understand the dynamics of re-epithelialization during wound closure, comparing injuries that
137 damage one or both epithelial layers.
138
139 **Amputations that damage the outer epidermal layer close through actin-based constriction**
140 Transverse amputations through the middle of the animal, separating the head from tail, have been
141 utilized as the dominant assay for whole-body regeneration across systems[14,47,48,50,51]. In *H. miamia,* a
142 typical transverse amputation aims to cut at the middle pigmentation stripe observable on the dorsal
143 surface of the worm, leaving behind a large gap with open epidermal edges around the wound. This
144 amputation halves some tissues (e.g. gut, nerve net, and musculature) and completely removes anterior
145 organs (e.g. pharynx and brain) from the posterior fragment. In addition to the biological process of
146 wound healing, these fragments therefore face different regenerative challenges: the head fragment
147 needs to regenerate the posterior tissues, whereas the tail fragment must regenerate anterior-specific
148 tissues and organs (Figure 2A).
149 We first amputated juvenile worms transversely below the pharynx, so that only the outer
150 epidermis (but not the pharyngeal epithelium) would be impacted by the injury. Consistent with previous
151 reports (cite), each fragment showed a rounded wound edge within 24 hours, suggesting successful
152 closure. Head fragments formed a pointed tail within 3 days (red arrowhead) and regained their original
153 shape within 5 days. The tail fragments took longer to regenerate but formed a visible blastema within 5
154 days (white arrowhead) and regained their original form within 10 days (Figure 2B). This temporal
155 trajectory reflects the regenerative challenge each fragment faces; the tail fragments need to replace
156 more cell types than their head counterparts. Although the brightfield imaging suggested that wound sites
157 had closed within 24 hours, we wanted to assess the cellular dynamics of the re-epithelialization process.
158 To track the dynamics of the outer epidermis during wound closure, we stained fragments with the
159 cytoskeletal dye SiR-actin at intermediate time points during the first 10 hours post-amputation (hpa).
160 Wounds from both head and tail fragments largely closed within 10 hpa, and both showed a strong
161 anisotropic enrichment of actin at the wound periphery, suggesting the formation of a supracellular
162 structure (Figure 2C-D). These observations appear consistent with a process of radial constriction,
163 where actin polarizes towards the wound edge and cells collectively pull towards the center of the wound

164 to minimize the size of the gap. Some wound edges displayed a smooth, continuous actin cable (yellow
165 arrowheads), implying the formation of an actomyosin purse-string[31,36], but others appear puckered (red
166 arrowheads), suggesting more of a general constrictive mechanism. Both head and tail fragments closed
167 their wounds at a similar rate; head wounds were more open than tail wounds at 3 hpa, but by 6 hpa we
168 found no difference between the two conditions (Figure 2D). Despite closure of the wound sites by 10
169 hpa, we observed visible differences in wound edges between 10 and 20 hpa. Closed wounds at 10 hpa
170 had visible seams where the epidermis was brought together (yellow arrows), but by 20 hpa there was no
171 detectable seam or wound edge (Figure 2E). This suggests a sustained re-epithelialization process even
172 after initial gap closure, where the epidermal cells continue to remodel their junctions and re-establish a
173 seamless epithelium.

174 To assess whether minor wounds utilize the same mechanisms of actomyosin contractility during
175 re-epithelialization as the transversely amputated wounds above, we performed 'pinch' wounds, where
176 fine-tipped forceps were used to pinch through the outer epidermis (Supplemental Figure 1A). These
177 wounds closed faster than wounds at transverse amputations and seemed to use a different cellular
178 mechanism. Instead of contracting across the wound gap, we observed the formation of polarized
179 protrusions within 5 minutes post-amputation, with the wound edges making contact and closing up within
180 1 hour (Supplemental Figure 1A). This is likely due to the much smaller distance between wounded
181 epidermal edges; in a pinch wound, the edges remain adjacent to each other, facilitating quick re-
182 epithelialization, but a transverse amputation causes a comparatively large wound gap that requires more
183 time to close.

184 Together, these results show that wounds that disrupt only one epithelial layer use shared
185 mechanisms of closure seen in other systems across contexts of regeneration, development, and repair.
186 Minor wounds with small gaps can close quickly and without the formation of supracellular structures,
187 whereas large amputations require the constriction of epithelial cells across the wound gap. We next
188 looked at the dynamics of closure in more complex wounds, specifically injuring both the outer epidermis
189 and the pharyngeal epithelium.

190

191 **Heterotypic epithelial bridges mediate the first step in multi-epithelial wound closure**

192 To investigate mechanisms of wound closure involving multiple epithelial layers, we performed injuries
193 that damage both the outer epidermis and the pharynx. We first cut animals in the sagittal plane,
194 separating the left half from the right, and observed wounds over a 10-day time course of regeneration
195 (Figure 3A-B). Interestingly, these animals were able to mostly restore their original shape within 5 days,
196 rounding themselves up without the formation of a visible blastema (Figure 3B). We therefore asked how
197 the epithelial layers facilitate the morphallactic processes of wound closure. Using SiR-actin labeling, we
198 amputated worms in the sagittal plane and observed the formation of striking, long cytoplasmic
199 protrusions that extend across the wound edge in the first 10 hpa. These protrusions originated from both
200 the outer epidermis and the pharyngeal epithelium, connecting across the middle of the wound (Figure
201 3C). To confirm that these cells were epithelial in nature, we utilized the *EpiA:RFP* transgenic line[52] and
202 detected protrusions in labeled cells within both the outer epidermis and the pharyngeal epithelium
203 (Supplementary Figure 2A-B). We were unable to visualize the basal side of cells forming these bridges,
204 but the extensions protruded from the apical surface of the cells - suggesting that these were new
205 structures and not movement of the homeostatic basal protrusions.
206 In sagittal wounds, epidermal cells showed signs of actin polarization within the first 3 hours post-
207 amputation (hpa), with small filopodial protrusions (5-10 μm) appearing in the outer epidermis oriented
208 towards the wound edge (Figure 3B). Long, thin extensions (>15 μm) emerged around 6 hpa, forming
209 more robustly by 10 hpa and connecting to projections originating from the pharyngeal epithelium (Figure
210 3D-E). This temporal pattern was consistent across animals, and 67% of fragments displayed at least one
211 connected bridge within 10 hpa (Figure 3E). Notably, protrusions were always detected first in the outer
212 epidermis, and protrusions from the pharyngeal epithelium were only visible after their counterparts
213 formed in the epidermis (Figure 3F). Corresponding with the number of bridges increasing between 6 and
214 10 hpa, the average bridge length increased significantly between time points (Figure 3G). This stepwise
215 process (polarization, extension, connection) is consistent with a model of collective cell migration[54,55], but
216 the lengths of these bridges (~30-100 μm) are reminiscent of specialized projections such as cytonemes
217 or tunneling nanotubes (which have been reported to reach up to 200 μm *in vivo*[56–58]). To the best of our
218 knowledge, structures like these heterotypic bridges have not been reported in wound closure literature,
219 and we therefore sought to further investigate this phenomenon.

220 The difference between transverse, contraction-based closure and sagittal, bridge-based closure
221 could be attributed to a variety of differences between the amputations other than the dual epithelial
222 layers, including (but not limited to): angle or orientation of amputation, size of the wound, or the extent of
223 regeneration required downstream of closure. We next asked whether heterotypic bridges occurred in
224 transverse amputations further up the anterior-posterior axis of the animal, upon injuries that impact both
225 epithelial layers by cutting through the pharynx. These wounds require closure in the same plane as the
226 transverse injuries reported above, but now include damage to the pharyngeal epithelium. When we
227 performed single and double transverse amputations through the pharynx, we observed robust
228 heterotypic bridges between the epidermis and the pharyngeal epithelium, similar to those seen in sagittal
229 amputations (Figure 3H-I). This bridge-based mechanism of closure is therefore not specific to the size or
230 the irregular wound geometry that comes from a sagittal amputation, but appear to instead be a more
231 general mechanism by which to close wounds when both epithelial layers are damaged.
232 Although these heterotypic bridges are unique in presentation, we reasoned that there must be a
233 substrate below these protrusions acting as a physical track for their extension. The extracellular matrix
234 (ECM) has been shown to be a key regulator of wound healing, acting as a dynamic substrate on which
235 cells can crawl and extend to complete re-epithelialization[42,59,60]. Given the known role of collagen IV in
236 wound closure[43,60–62], we identified a putative ortholog in the *H. miamia* transcriptome and made a custom
237 antibody (see Methods). Using this antibody, we performed immunofluorescence staining to assess the
238 localization of collagen IV and detected its expression solely under the pharyngeal epithelium
239 (Supplemental Figure 2C-D). Next, we asked whether collagen IV was remodeled during wound closure
240 as the pharyngeal epithelium is extending its protrusions. We performed immunofluorescence on 10 hpa
241 sagittal fragments and observed strong co-localization of collagen IV specifically underneath pharyngeal
242 extensions. Collagen signal was never detected in areas without protrusions, suggesting that nascent
243 collagen is being deposited underneath the pharyngeal epithelium as it is forming wound-induced bridges
244 (Supplemental Figure 2E). The same pattern was observed after double transverse amputation,
245 suggesting a shared mechanism regardless of wound geometry (Supplemental Figure 2F). These data
246 implicate collagen IV as a substrate for epithelial bridges, likely providing physical support for protrusions
247 as they extend across the wound site. Although our antibody specifically labels the collagen underneath

248 the pharyngeal epithelium, we speculate that a similar process is occurring underneath protrusions
249 coming from outer epidermal cells.
250 Taken together, these findings reveal the presence of heterotypic cellular bridges between
251 epithelial layers during wound closure, which emerge within the first 10 hours post-amputation. Tissue-
252 specific collagen is remodeled during the extension of pharyngeal protrusions, and bridges are observed
253 across different amputation geometries that injure multiple epithelial layers. We therefore hypothesized
254 that these heterotypic interactions act as an intermediate step in large-scale multi-epithelial wound
255 closure, possibly minimizing tissue loss and/or maintaining tissue identity prior to full re-epithelialization.
256 To the best of our knowledge, this phenomenon appears to be a novel healing mechanism, and we
257 sought to understand how these heterotypic interactions relate to the rest of the wound healing process.
258
259 **Wound closure involving multiple epithelial tissues utilizes distinct but temporally overlapping**
260 **cellular mechanisms**
261 The bridges described above represent a transient phase in wound closure, emerging within the first 10
262 hours post-amputation (hpa). In order for the animal to heal fully, the sagittal fragments must undergo
263 continued remodeling to re-establish their original shape. Our regeneration time course demonstrated that
264 sagittal amputations in *H. miamia* do not form a blastema, but instead slowly round up over the course of
265 70 hours (Figure 3B). To gain further insight into the cellular processes driving this morphogenetic
266 movement, we stained sagittal fragments with SiR-actin over the course of 70 hours post-amputation
267 (hpa) (Figure 4A). We observed that these animals healed through a two-step process: as described
268 above, the outer epidermis first connects to the pharyngeal epithelium within the first 10 hpa, followed by
269 the posterior end closing itself up through what appears to be a combination of epithelial crawling and
270 zippering. Both of these cellular movements are well-described in other systems, and here we see a
271 similar gradual closure of the outer epidermis as it meets and re-epithelializes with the epidermis from the
272 other side of the animal.
273 As the posterior ends are closing, sagittally-cut animals round their bodies up to re-form their
274 cylindrical shapes. The two processes we observexd (heterotypic bridges and homotypic re-
275 epithelialization) occur in a stepwise but overlapping sequence, where all fragments first form visible

276 bridges, then display both bridges and posterior closure, and finally end with just posterior re-
277 epithelialization (Figure 4B-C). All animals had an open body shape between 0-10 hpa, characterized by
278 a splayed pharynx and separated dorsal and ventral halves. At 20 hpa, we began to see rounding of the
279 fragments, with the outer epidermal edges curling over the pharynx towards each other. While some
280 animals closed as early as 30 hpa, virtually all animals completed this closure by 70 hpa (Figure 4B-D).
281 Here, closure is defined by the original dorsal and ventral edges completely meeting at the seam of the
282 wound, forming a cylinder with the pharynx on the inside and the epidermis on the outside. We speculate
283 that this rounding process is aiding the posterior re-epithelialization by bringing the wound edges
284 together.

285 To rule out that this dual closure mechanism was unique to the sagittal amputation, we next
286 asked whether similar processes occurred in transverse injuries that form heterotypic bridges. We
287 amputated animals both once (single transverse) and twice (donut) through the pharynx and tracked
288 regeneration. The single transverse fragments followed a similar regeneration trajectory as their
289 counterparts amputated below the pharynx (Figure 2B), although the differences in fragment size
290 correlated with different temporal dynamics (Supplemental Figure 3A). The donut fragments formed
291 blastemas on both anterior and posterior ends, regenerating all missing structures despite the severity of
292 the injury (Supplemental Figure 3B). To track the dynamics of wound closure in these amputations, we
293 fixed animals at intermediate time points and stained fragments with SiR-actin. Unlike the sagittal
294 fragments, the transverse fragments didn't zipper after the formation of bridges, but instead contracted
295 their outer epidermis over the wound site in a process that appeared similar to the single-epithelial
296 transverse amputations (Supplemental Figure 3C-D, Figure 2B).

297 These observations suggest that while the exact mechanism of wound closure is determined by a
298 combination of factors, injuries involving both epithelial layers follow a coordinated two-step process.
299 First, heterotypic protrusions bridge the wound gap between the two epithelial layers, followed by the
300 outer epidermis re-epithelializing with itself. We next asked how cell and tissue contractility was involved
301 in these mechanisms of wound closure, seeking to combine the characterization of these processes with
302 functional perturbations.
303

304 **Muscle contraction is necessary for both heterotypic wound closure and downstream**
305 **morphogenetic movements**
306 Contraction of muscle at the wound site is an essential component of wound closure in both vertebrates
307 and invertebrates, driving physical and biochemical events through the generation of mechanical
308 force[22,26,29,63]. Because of the close proximity of epithelial cells to underlying muscle in *H. miamia* (Figure
309 1G), we next asked whether muscle contraction was involved in wound closure. *H. miamia* have an
310 extensive network of muscle throughout their bodies (Figure 5A), and we utilized Tropomyosin
311 immunofluorescence to visualize how muscle was reorganized during single and dual epithelial wound
312 closure. In transverse wounds (both head and tail), muscle was largely absent from the wound site itself
313 but was instead present at the periphery of the wound edge as it shrank (Figure 5B). In contrast, sagittal
314 wounds contain parenchymal muscle fibers that link the outer epidermis to the pharyngeal epithelium,
315 coming together as the animal rounds up (Figure 5C). We hypothesized that this difference in muscle
316 organization might influence the closure mechanisms used by each fragment, and asked whether muscle
317 contraction was required for each type of wound closure.
318 To test the functional role of muscle contraction, we anesthetized amputated animals in 0.1%
319 tricaine, which blocks neural action potentials[64] and effectively inhibits muscle contraction in *H. miamia*
320 (Video 1). In the presence of tricaine, single epithelial wound closure in transverse amputations occurs at
321 the same rate as controls (Figure 5C-D), indicating that the epidermis is capable of constricting and re-
322 epithelializing without the aid of muscle contraction. Animals with multi-epithelial wounds, on the other
323 hand, are incapable of forming heterotypic bridges without muscle contraction (Figure 5E-G). We
324 observed some polarization and formation of small protrusions from the epidermis and pharyngeal
325 epithelium, but no bridges ever formed in tricaine-treated animals (Figure 5F). The requirement of muscle
326 contraction for the formation of heterotypic bridges was consistent across all multi-epithelial injuries
327 (Supplemental Figure 4A-B), suggesting a shared mechanism.
328 We performed time courses with tricaine treatment to determine whether muscle contraction was
329 only necessary for the initiation of the heterotypic bridges or whether muscle contraction was needed for
330 both their formation and maintenance (Supplemental Figure 4C). Animals treated with tricaine for 10
331 hours, then placed in sea water for 20 hours, closed wounds at a similar rate to controls. In contrast,

332 animals that were in sea water for 10 hours and then placed in tricaine for 20 hours were
333 indistinguishable from animals treated with tricaine for all 30 hours (Supplemental Figure 4D-E). This
334 indicates both that persistent muscle contraction is necessary for the maintenance of heterotypic bridges,
335 and that animals can fully recover after anesthetization.
336 Interestingly, muscle contraction is only required for the participation of the outer epidermis in
337 forming heterotypic bridges. In the presence of tricaine, the pharyngeal epithelium still formed extensions
338 and spread to try and cover the wound site (Supplemental Figure 4F-G). While the exact function is not
339 yet clear, these data implicate muscle contraction as a necessary driver of multi-epithelial wound closure.
340 This contraction may be involved in generating tension, inducing mechanical or biochemical signals,
341 and/or physically bringing the wound edges together to allow contact between the epithelia. Without
342 muscle-generated mechanical force, the outer epidermis cannot generate or maintain long protrusions to
343 form heterotypic bridges, and the wound closure process stalls and collapses.
344 Together, these findings highlight the importance of muscle contractility in mediating cellular
345 events during multi-epithelial wound closure. To distinguish between the role of tissue-scale mechanical
346 forces generated by muscle and the cell-intrinsic forces required for protrusive activity and wound closure,
347 we next assessed the role of actomyosin contractility in wound closure.
348
349 **Types of wound closure are differentially regulated by actomyosin contractility**
350 Actomyosin contractility is generated through the interactions of non-muscle myosin with actin, producing
351 mechanical forces within cells that enable cytoskeletal rearrangements and cellular movements[65–67].
352 While actomyosin contractility is broadly implicated in wound closure across species, we wanted to know
353 how its role varied across injury types in *H. miamia*. We treated amputated animals with the inhibitor
354 blebbistatin, which inhibits the ATPase activity of myosin and blocks actomyosin contractility[68,69]. In the
355 presence of blebbistatin, transverse wounds (which only disrupt the outer epidermis) closed at
356 comparable speeds to control conditions but appeared to switch towards more crawling-dominant
357 mechanisms (Figure 6A-C): instead of the contractile rings seen in control fragments, we detected
358 protrusions around the wound edge and saw individual cells crawling across the wound site (Figure 6C).

359 These data indicate that protrusion-based mechanisms are sufficient to accomplish wound closure in
360 blebbistatin-treated conditions.

361 We next asked how actomyosin contractility was involved in multi-epithelial wound closure. In
362 contrast to the mild phenotype in single epithelial wounds, we observed significant closure defects in the
363 blebbistatin-treated animals. Blebbistatin treatment eliminated the formation of stable heterotypic bridges
364 in sagittal fragments at 10 hpa (Figure 6D). We observed short protrusions emerging from both the outer
365 epidermis and pharyngeal epithelium, but their orientation appeared more random than control fragments,
366 forming multiple protrusions rather than connected bridges (Figure 6E, Supplemental Figure 5A). These
367 data indicate that actomyosin contractility is essential for the extension of long protrusions across the
368 wound edge to form heterotypic bridges. This contractility may be important in the stabilization of
369 protrusions as they extend, the application of pulling forces to bring the epithelia together, and/or the
370 stabilization of nascent adhesions at heterotypic interfaces[34,39,66,70–72]. Without this contractility, small
371 protrusions can form, but they ultimately lack the necessary force to form bridges.

372 Contrasting with the inhibition of heterotypic bridges, we observed an acceleration of epidermal
373 re-epithelialization in blebbistatin-treated animals. In control conditions, the zippering up of the posterior
374 end began around ~20-30 hours after amputation, after the formation of heterotypic bridges at the anterior
375 end (Figure 4D). In contrast, animals treated with blebbistatin showed posterior closure as early as 10
376 hpa, even in the absence of heterotypic bridges (Figure 6F-H). This phenotype is consistent with that
377 seen in other systems, in which the reduction of junctional tension 'loosens' the epithelial sheet and
378 allows epidermal cells to move more freely relative to each other[30,68,73]. By 20 hpa, blebbistatin-treated
379 animals showed robust closure of the outer epidermis, but no heterotypic bridges and no rounding of the
380 pharyngeal epithelium. Prolonged treatment with blebbistatin for 50 hours, however, led to reduced tissue
381 integrity in the epidermis, manifesting first as holes between cells and leading to eventual epidermal
382 ruptures (Figure 6H). The presumed decrease in junctional tension that enabled accelerated cell
383 spreading also prevented the maintenance of strong junctions between cells, resulting in a weakened
384 epidermal layer that was unable to withstand the mechanical demands of healing and regeneration.

385 Lastly, we assessed whether this phenotype was reversible and if the epidermis could re-
386 establish its integrity after accelerated re-epithelialization. We placed blebbistatin-treated animals in fresh

387 sea water after a 30-hour incubation for either 20 (50 hpa time point) or 40 (70 hpa time point) hours,
388 comparing directly to control animals and animals left in blebbistatin for the full time course
389 (Supplementary Figure 5B). Animals that were placed in fresh ASW for 20h were rounder than their
390 counterparts that remained in blebbistatin, suggesting a re-entry into the typical morphogenetic trajectory
391 (Supplementary Figure 5C-D). Animals that were placed in fresh ASW for 40 hours were able to
392 completely recover, resembling the control animals at 70 hpa (Supplementary Figure 5C-D). This
393 suggests that while prolonged blebbistatin treatment will lead to a loss of epidermal integrity, the animals
394 will restore junctional tension after removal of the drug, continuing the re- wound closure process.
395

396 **DISCUSSION**

397 In this study, we demonstrate that the acoel *Hofstenia miamia* uses context-dependent wound healing,
398 employing complementary and overlapping mechanisms of re-epithelialization to repair wounds prior to
399 whole-body regeneration. Wounds disrupting only one tissue use rapid and conserved closure
400 mechanisms, similar to wound closure in other species. In control conditions, these wounds primarily rely
401 on radial constriction of the epidermis, but in contractility-inhibited conditions the epidermal cells shift
402 mechanisms and close through crawling. Multi-epithelial wounds close through a combination of novel
403 heterotypic bridges and homotypic epithelial zippering, requiring both actomyosin-generated tension and
404 muscle contraction to drive coordinated tissue movements. In conditions of reduced global contractility,
405 other closure mechanisms are transiently upregulated, but ultimately fail to restore long-term tissue
406 integrity unless contractility is restored. Mechanisms of wound closure in *H. miamia* are therefore not
407 uniform or discrete processes, but are instead highly dynamic and cooperative, shifting in response to
408 both intrinsic and extrinsic factors.

409 The heterotypic bridges described here are, to the best of our knowledge, a novel wound-induced
410 response. Heterotypic contacts have been described in other systems as mechanisms by which tissue
411 boundaries are maintained during development[75–79], but filopodial matching that has been observed[79]
412 appears distinct from these bridges both in size and duration. Instead of fast filopodial probing between
413 proximal cells to form the proper adhesive complexes, the bridges observed in *H. miamia* are long (>50
414 um) and visible for at least 10 hours. At present, we cannot rule out the possibility that these bridges are

415 dynamic due to a lack of live imaging, but their length paired with the clear progression of formation
416 (polarization of actin, followed by short protrusions, then connected bridges) suggests some temporal
417 stability. Although they differ in presentation, it's possible that these heterotypic contacts are functioning
418 similarly to maintain tissue borders. During regeneration, injuries that damage both epithelial layers must
419 preserve both tissue identity and orientation, ultimately restoring the 'tube within a tube' anatomy.
420 Because we do not yet have tissue-specific labeling to differentiate between the epithelial layers, we don't
421 know how the bridges resolve during secondary closure. However, the framework presented here will set
422 the stage for future studies, including better visualization of cellular interactions, identification of adhesion
423 and migration machinery, the role of signaling pathways, and more.
424 When assessing the dynamics of these heterotypic interactions, we observed that the outer
425 epidermis requires muscle contraction to form stable protrusions, but the pharyngeal epithelium can
426 spread across the wound even in the absence of epidermal contributions. This phenotype could be due to
427 intrinsic differences in the epithelia; for example, perhaps the pharyngeal epithelium has intrinsic cell
428 motility machinery that is primed for migration regardless of external forces. In the animal's undamaged
429 configuration, the pharyngeal epithelium is surrounded by rings of pharyngeal muscle. It's possible that
430 when that muscle is damaged, the epithelial cells are now able to spread and crawl across the wound
431 site. In contrast, the outer epidermal cells may be more stable and require assistance from muscle
432 contraction to bring the two layers close enough to form stable adhesions. The differences between the
433 epithelial responses could also be due to their extrinsic interactions. The epithelial cells in *H. miamia* are
434 anatomically unique, lacking a flat basal surface as is typically observed in most animal epithelia and
435 instead forming long projections that end in close proximity to muscle. Electron microscopy in acoels has
436 failed to identify a visible basement membrane underneath the outer epidermis[74], but the composition of
437 extracellular matrix (ECM) in *H. miamia* has not been studied. It is therefore unclear whether the ECM is
438 adhering to protrusions in a punctate fashion, if there is ECM surrounding muscle fibers, if there is a thin
439 layer of ECM in between cellular protrusions, or any other organization. Using a custom antibody in this
440 study, we demonstrate that there is tissue-specific collagen underneath the pharyngeal epithelial cells,
441 and that collagen is present underneath their wound-induced protrusions. We did not observe this
442 collagen underneath the outer epidermis, but a similar mechanism could be occurring with a different

443 extracellular matrix protein, perhaps one whose remodeling is mechanosensitive. Differences in ECM
444 stiffness and composition could affect the mechanical response of each tissue, as well as differences in
445 regular tensile loads. It has also been shown in other systems that wound-induced muscle contraction
446 triggers the release of matrix remodeling proteins[42,59], which could be necessary for epidermal cells to
447 extend far enough to reach their pharyngeal epithelial counterparts. Future studies will need to further
448 characterize the *H. miamia* ECM and its dynamics to distinguish between these hypotheses.
449 The difference in wound closure strategies across injury types raises several questions about the
450 connection between healing and regeneration. It seems probable that different forms of wound closure
451 correlate with different cellular and molecular environments in regenerating fragments, whether through
452 biochemical and/or mechanical events associated with re-epithelialization. Future work will be required to
453 test whether different closure strategies have functional consequences for downstream tissue
454 regeneration, whether healing and regeneration are distinct and nonoverlapping biological processes, and
455 whether other species capable of whole-body regeneration utilize distinct mechanisms to heal different
456 types of wounds.
457
458

459 **REFERENCES**

460 1. Bely, A. E. & Nyberg, K. G. Evolution of animal regeneration: re-emergence of a field. *Trends Ecol.*
461 *Evol.* **25**, 161–170 (2010).
462 2. Post, Y. & Clevers, H. Defining Adult Stem Cell Function at Its Simplest: The Ability to Replace Lost
463 Cells through Mitosis. *Cell Stem Cell* **25**, 174–183 (2019).
464 3. Abreu-Blanco, M. T., Verboon, J. M., Liu, R., Watts, J. J. & Parkhurst, S. M. *Drosophila* embryos close
465 epithelial wounds using a combination of cellular protrusions and an actomyosin purse string. *J. Cell*
466 *Sci.* **125**, 5984–5997 (2012).
467 4. Fernandez-Gonzalez, R. & Zallen, J. A. Wounded cells drive rapid epidermal repair in the early
468 *Drosophila* embryo. *Mol. Biol. Cell* **24**, 3227–3237 (2013).
469 5. Rothenberg, K. E. & Fernandez-Gonzalez, R. Forceful closure: cytoskeletal networks in embryonic
470 wound repair. *Mol. Biol. Cell* **30**, 1353–1358 (2019).
471 6. Begnaud, S., Chen, T., Delacour, D., Mège, R.-M. & Ladoux, B. Mechanics of epithelial tissues during
472 gap closure. *Curr. Opin. Cell Biol.* **42**, 52–62 (2016).
473 7. Lim, S. E., Vicente-Munuera, P. & Mao, Y. Forced back into shape: Mechanics of epithelial wound
474 repair. *Curr. Opin. Cell Biol.* **87**, 102324 (2024).
475 8. Jacinto, A., Martinez-Arias, A. & Martin, P. Mechanisms of epithelial fusion and repair. *Nat. Cell Biol.*
476 **3**, E117–E123 (2001).
477 9. Chablais, F. & Jaźwińska, A. IGF signaling between blastema and wound epidermis is required for fin
478 regeneration. *Development* **137**, 871–879 (2010).
479 10. Scimone, M. L., Cloutier, J. K., Maybrun, C. L. & Reddien, P. W. The planarian wound epidermis gene
480 equinox is required for blastema formation in regeneration. *Nat. Commun.* **13**, 2726 (2022).
481 11. Aztekin, C. Tissues and Cell Types of Appendage Regeneration: A Detailed Look at the Wound
482 Epidermis and Its Specialized Forms. *Front. Physiol.* **12**, 771040 (2021).
483 12. Aztekin, C. *et al.* Identification of a regeneration-organizing cell in the *Xenopus* tail. *Science* **364**,
484 653–658 (2019).
485 13. Bideau, L., Kerner, P., Hui, J., Vervoort, M. & Gazave, E. Animal regeneration in the era of
486 transcriptomics. *Cell. Mol. Life Sci.* **78**, 3941–3956 (2021).

487 14. Amiel, A. *et al.* Characterization of Morphological and Cellular Events Underlying Oral Regeneration
488 in the Sea Anemone, Nematostella vectensis. *Int. J. Mol. Sci.* **16**, 28449–28471 (2015).
489 15. Ben Khadra, Y. *et al.* Wound repair during arm regeneration in the red starfish *E chinaster sepositus*.
490 *Wound Repair Regen.* **23**, 611–622 (2015).
491 16. Cheung, S. *et al.* Systemic coordination of whole-body tissue remodeling during local regeneration in
492 sea anemones. *Dev. Cell* S153458072400666X (2024) doi:10.1016/j.devcel.2024.11.001.
493 17. Lust, K. *et al.* Single-cell analyses of axolotl telencephalon organization, neurogenesis, and
494 regeneration. *Science* **377**, eabp9262 (2022).
495 18. Kassmer, S. H., Nourizadeh, S. & De Tomaso, A. W. Cellular and molecular mechanisms of
496 regeneration in colonial and solitary Ascidians. *Dev. Biol.* **448**, 271–278 (2019).
497 19. Kamran, Z. *et al.* In vivo imaging of epithelial wound healing in the cnidarian Clytia hemisphaerica
498 demonstrates early evolution of purse string and cell crawling closure mechanisms. *BMC Dev. Biol.*
499 **17**, 17 (2017).
500 20. Ramon-Mateu, J., Ellison, S. T., Angelini, T. E. & Martindale, M. Q. Regeneration in the ctenophore
501 Mnemiopsis leidyi occurs in the absence of a blastema, requires cell division, and is temporally
502 separable from wound healing. *BMC Biol.* **17**, 80 (2019).
503 21. Spiegelman, M. & Dudley, P. L. Morphological stages of regeneration in the planarian *Dugesia*
504 *tigrina* : A light and electron microscopic study. *J. Morphol.* **139**, 155–183 (1973).
505 22. Shaw, T. J., Osborne, M., Ponte, G., Fiorito, G. & Andrews, P. L. R. Mechanisms of wound closure
506 following acute arm injury in Octopus vulgaris. *Zool. Lett.* **2**, 8 (2016).
507 23. Donaldson, D. J. & Dunlap, M. K. Epidermal cell migration during attempted closure of skin wounds in
508 the adult newt: Observations based on cytochalasin treatment and scanning electron microscopy. *J.*
509 *Exp. Zool.* **217**, 33–43 (1981).
510 24. Huang, T. *et al.* Re-epithelialization of large wound in paedomorphic and metamorphic axolotls. *J.*
511 *Morphol.* **278**, 228–235 (2017).
512 25. Zattara, E. E., Turlington, K. W. & Bely, A. E. Long-term time-lapse live imaging reveals extensive cell
513 migration during annelid regeneration. *BMC Dev. Biol.* **16**, 6 (2016).

514 26. Chandebois, R. THE DYNAMICS OF WOUND CLOSURE AND ITS ROLE IN THE PROGRAMMING
515 OF PLANARIAN REGENERATION. II - DISTALIZATION. *Dev. Growth Differ.* **22**, 693–704 (1980).
516 27. Belacortu, Y. & Paricio, N. *Drosophila* as a model of wound healing and tissue regeneration in
517 vertebrates. *Dev. Dyn.* **240**, 2379–2404 (2011).
518 28. Brewer, C. M. *et al.* Adaptations in Hippo-Yap signaling and myofibroblast fate underlie scar-free ear
519 appendage wound healing in spiny mice. *Dev. Cell* **56**, 2722-2740.e6 (2021).
520 29. Valero, C., Javierre, E., García-Aznar, J. M. & Gómez-Benito, M. J. A Cell-Regulatory Mechanism
521 Involving Feedback between Contraction and Tissue Formation Guides Wound Healing Progression.
522 *PLoS ONE* **9**, e92774 (2014).
523 30. Tetley, R. J. *et al.* Tissue fluidity promotes epithelial wound healing. *Nat. Phys.* **15**, 1195–1203 (2019).
524 31. Bement, W. M., Mandato, C. A. & Kirsch, M. N. Wound-induced assembly and closure of an
525 actomyosin purse string in Xenopus oocytes. *Curr. Biol.* **9**, 579–587 (1999).
526 32. Nobes, C. D. & Hall, A. Rho, Rac, and Cdc42 GTPases regulate the assembly of multimolecular focal
527 complexes associated with actin stress fibers, lamellipodia, and filopodia. *Cell* **81**, 53–62 (1995).
528 33. Henson, J. H. *et al.* Wound Closure in the Lamellipodia of Single Cells: Mediation by Actin
529 Polymerization in the Absence of an Actomyosin Purse String. *Mol. Biol. Cell* **13**, 1001–1014 (2002).
530 34. Tang, V. W. Cell–cell adhesion interface: orthogonal and parallel forces from contraction, protrusion,
531 and retraction. *F1000Research* **7**, 1544 (2018).
532 35. Da Costa, A. D. S. *et al.* Fibroblasts Close a Void in Free Space by a Purse-String Mechanism. *ACS*
533 *Appl. Mater. Interfaces* **14**, 40522–40534 (2022).
534 36. Rodriguez-Diaz, A. *et al.* Actomyosin purse strings: Renewable resources that make morphogenesis
535 robust and resilient. *HFSP J.* **2**, 220–237 (2008).
536 37. Ehrlich, H. P. Wound closure: evidence of cooperation between fibroblasts and collagen matrix. *Eye*
537 **2**, 149–157 (1988).
538 38. Basan, M., Elgeti, J., Hannezo, E., Rappel, W.-J. & Levine, H. Alignment of cellular motility forces
539 with tissue flow as a mechanism for efficient wound healing. *Proc. Natl. Acad. Sci.* **110**, 2452–2459
540 (2013).

541 39. Vedula, S. R. K. *et al.* Mechanics of epithelial closure over non-adherent environments. *Nat.*
542 *Commun.* **6**, 6111 (2015).
543 40. Xu, H. *et al.* Geometry-mediated bridging drives nonadhesive stripe wound healing. *Proc. Natl. Acad.*
544 *Sci.* **120**, e2221040120 (2023).
545 41. Pascolini, R., Tei, S., Vagnetti, D. & Bondi, C. Epidermal cell migration during wound healing in
546 Dugesia lugubris: Observations based on scanning electron microscopy and treatment with
547 cytochalasin. *Cell Tissue Res.* **236**, (1984).
548 42. Chakraborty, S. *et al.* Agrin-Matrix Metalloproteinase-12 axis confers a mechanically competent
549 microenvironment in skin wound healing. *Nat. Commun.* **12**, 6349 (2021).
550 43. Brauer, E. *et al.* Collagen Fibrils Mechanically Contribute to Tissue Contraction in an In Vitro Wound
551 Healing Scenario. *Adv. Sci.* **6**, 1801780 (2019).
552 44. Yannas, I. V. & Tzeranis, D. S. Mammals fail to regenerate organs when wound contraction drives
553 scar formation. *Npj Regen. Med.* **6**, 39 (2021).
554 45. Kimura, S. & Tsuji, T. Mechanical and Immunological Regulation in Wound Healing and Skin
555 Reconstruction. *Int. J. Mol. Sci.* **22**, 5474 (2021).
556 46. Nier, V. *et al.* Tissue fusion over nonadhering surfaces. *Proc. Natl. Acad. Sci.* **112**, 9546–9551 (2015).
557 47. Srivastava, M., Mazza-Curll, K. L., van Wolfswinkel, J. C. & Reddien, P. W. Whole-Body Acoel
558 Regeneration Is Controlled by Wnt and Bmp-Admp Signaling. *Curr. Biol.* **24**, 1107–1113 (2014).
559 48. Raz, A. A., Srivastava, M., Salvamoser, R. & Reddien, P. W. Acoel regeneration mechanisms indicate
560 an ancient role for muscle in regenerative patterning. *Nat. Commun.* **8**, 1260 (2017).
561 49. Srivastava, M. Studying development, regeneration, stem cells, and more in the acoel Hofstenia
562 miamia. in *Current Topics in Developmental Biology* vol. 147 153–172 (Elsevier, 2022).
563 50. Hulett, R. E. *et al.* Acoel single-cell atlas reveals expression dynamics and heterogeneity of adult
564 pluripotent stem cells. *Nat. Commun.* **14**, 2612 (2023).
565 51. Reddien, P. W. Positional Information and Stem Cells Combine to Result in Planarian Regeneration.
566 *Cold Spring Harb. Perspect. Biol.* a040717 (2021) doi:10.1101/cshperspect.a040717.
567 52. Ricci, L. & Srivastava, M. Transgenesis in the acoel worm Hofstenia miamia. *Dev. Cell* **56**, 3160-
568 3170.e4 (2021).

569 53. Doerr, S., Zhou, P. & Ragkousi, K. Origin and development of primary animal epithelia. *BioEssays* **46**,
570 2300150 (2024).
571 54. Friedl, P. & Gilmour, D. Collective cell migration in morphogenesis, regeneration and cancer. *Nat.*
572 *Rev. Mol. Cell Biol.* **10**, 445–457 (2009).
573 55. Macabenta, F. & Stathopoulos, A. Sticking to a plan: adhesion and signaling control spatial
574 organization of cells within migrating collectives. *Curr. Opin. Genet. Dev.* **57**, 39–46 (2019).
575 56. Patel, A. *et al.* Cytonemes coordinate asymmetric signaling and organization in the Drosophila
576 muscle progenitor niche. *Nat. Commun.* **13**, 1185 (2022).
577 57. Daly, C. A., Hall, E. T. & Ogden, S. K. Regulatory mechanisms of cytoneme-based morphogen
578 transport. *Cell. Mol. Life Sci.* **79**, 119 (2022).
579 58. Caviglia, S. & Ober, E. A. Non-conventional protrusions: the diversity of cell interactions at short and
580 long distance. *Curr. Opin. Cell Biol.* **54**, 106–113 (2018).
581 59. Sakar, M. S. *et al.* Cellular forces and matrix assembly coordinate fibrous tissue repair. *Nat.*
582 *Commun.* **7**, 11036 (2016).
583 60. Naba, A. Mechanisms of assembly and remodelling of the extracellular matrix. *Nat. Rev. Mol. Cell*
584 *Biol.* **25**, 865–885 (2024).
585 61. Ehrlich, H. P. & Hunt, T. K. Collagen Organization Critical Role in Wound Contraction. *Adv. Wound*
586 *Care* **1**, 3–9 (2012).
587 62. Xue, M. & Jackson, C. J. Extracellular Matrix Reorganization During Wound Healing and Its Impact
588 on Abnormal Scarring. *Adv. Wound Care* **4**, 119–136 (2015).
589 63. Li, B. & Wang, J. H.-C. Fibroblasts and myofibroblasts in wound healing: Force generation and
590 measurement. *J. Tissue Viability* **20**, 108–120 (2011).
591 64. Attili, S. & Hughes, S. M. Anaesthetic Tricaine Acts Preferentially on Neural Voltage-Gated Sodium
592 Channels and Fails to Block Directly Evoked Muscle Contraction. *PLoS ONE* **9**, e103751 (2014).
593 65. Brunet, T. Cell contractility in early animal evolution. *Curr. Biol.* **33**, R966–R985 (2023).
594 66. Röper, K. Integration of Cell–Cell Adhesion and Contractile Actomyosin Activity During
595 Morphogenesis. in *Current Topics in Developmental Biology* vol. 112 103–127 (Elsevier, 2015).

596 67. Weißenbruch, K. & Mayor, R. Actomyosin forces in cell migration: Moving beyond cell body retraction.
597 *BioEssays* **46**, 2400055 (2024).
598 68. Liu, Z. *et al.* Blebbistatin inhibits contraction and accelerates migration in mouse hepatic stellate
599 cellsbph_477304..315. *Br. J. Pharmacol.* (2010).
600 69. Holz, O., Apel, D. & Hassel, M. Alternative pathways control actomyosin contractility in
601 epitheliomuscle cells during morphogenesis and body contraction. *Dev. Biol.* **463**, 88–98 (2020).
602 70. Li, J. X. H., Tang, V. W., Boateng, K. A. & Brieher, W. M. Cadherin puncta are interdigitated dynamic
603 actin protrusions necessary for stable cadherin adhesion. *Proc. Natl. Acad. Sci.* **118**, e2023510118
604 (2021).
605 71. Padhi, A. *et al.* Force-exerting perpendicular lateral protrusions in fibroblastic cell contraction.
606 *Commun. Biol.* **3**, 390 (2020).
607 72. Miroshnikova, Y. A. *et al.* Adhesion forces and cortical tension couple cell proliferation and
608 differentiation to drive epidermal stratification. *Nat. Cell Biol.* **20**, 69–80 (2018).
609 73. Cartagena-Rivera, A. X., Van Itallie, C. M., Anderson, J. M. & Chadwick, R. S. Apical surface
610 supracellular mechanical properties in polarized epithelium using noninvasive acoustic force
611 spectroscopy. *Nat. Commun.* **8**, 1030 (2017).
612 74. Dorey, A. E. The organization and replacement of the epidermis in acoelous turbellarians. *J. Cell Sci.*
613 **S3-106**, 147–172 (1965).
614 75. Batlle, E. & Wilkinson, D. G. Molecular Mechanisms of Cell Segregation and Boundary Formation in
615 Development and Tumorigenesis. *Cold Spring Harb. Perspect. Biol.* **4**, a008227–a008227 (2012).
616 76. Moore, R. E., Clarke, J. & Alexandre, P. Protrusion-Mediated Signaling Regulates Patterning of the
617 Developing Nervous System. *Front. Cell Dev. Biol.* **8**, 579073 (2020).
618 77. Katsunuma, S. *et al.* Synergistic action of nectins and cadherins generates the mosaic cellular
619 pattern of the olfactory epithelium. *J. Cell Biol.* **212**, 561–575 (2016).
620 78. Canty, L., Zarour, E., Kashkooli, L., François, P. & Fagotto, F. Sorting at embryonic boundaries
621 requires high heterotypic interfacial tension. *Nat. Commun.* **8**, 157 (2017).
622 79. Zhang, S., Amourda, C., Garfield, D. & Saunders, T. E. Selective Filopodia Adhesion Ensures Robust
623 Cell Matching in the Drosophila Heart. *Dev. Cell* **46**, 189-203.e4 (2018).

80. Hulett, R. E., Potter, D. & Srivastava, M. Neural architecture and regeneration in the acoel *Hofstenia miamia*. *Proc. R. Soc. B Biol. Sci.* **287**, 20201198 (2020).

627 **MATERIALS AND METHODS**

628 ***H. miamia* strains and husbandry**

629 Adult worms were housed in artificial sea water (ASW) (37 ppt, pH 7.70-8.00) in plastic boxes within 21ºC
630 incubators. Embryos were collected from adult boxes and placed into petri dishes for development. Once
631 hatched, juvenile worms were transferred to tanks for post-embryonic growth. All animals were fed twice a
632 week; adult worms were fed brine shrimp (Artemia, Brine Shrimp Direct) and juvenile hatchlings were fed
633 rotifers (*Brachionus plicatilis*, Reed Mariculture). *EpiA:RFP* worms were generated as previously
634 described[52].

635

636 **Amputations and sample preparation**

637 Juvenile worms were isolated and starved for 1-2 weeks prior to use to minimize autofluorescence of
638 ingested food. For regeneration experiments, animals were placed in 1mg/mL ethyl 3-aminobenzoate,
639 methanesulfonic acid ("tricaine", stock solution 5mg/mL of ASW) (Thermo Fisher, AC118000100) in ASW
640 in a petri dish for 3-5 minutes until they stopped swimming, then amputated using a scalpel. After
641 amputation, fragments were transferred to a dish containing fresh ASW until their designated time point.
642 For fixation, animals were placed in 4% paraformaldehyde (PFA) (Thomas Scientific, C993M31) in ASW
643 for 1 hour at room temperature. The PFA was removed and animals were washed with PBST (PBS +
644 0.1% Triton-X-100) three times prior to immunofluorescence staining. For pinch wounds, animals were
645 grasped with fine-tip forceps, then allowed to recover in ASW prior to fixation. For transverse and donut
646 cuts, animals were cut once or twice transversely, then transferred to fresh ASW until their designated
647 time point. For single transverse wounds, animals were cut transversely once again, right above the
648 previous cut, to remove the wound site for imaging. These fragments were then immediately fixed in 4%
649 PFA in ASW.

650

651 **Small molecule inhibitors and treatment with anesthetics**

652 For small molecule inhibitor experiments, animals were first amputated as described above, then flushed
653 with ASW to remove tricaine prior to incubation in designated inhibitors. Animals were left in inhibitor for
654 3-70 hours, depending on the experiment. Blebbistatin (Sigma-Aldrich, B0560) was dissolved in DMSO

655 per manufacturer instructions, then diluted in ASW for use at 25µM. DMSO control treatments used an
656 equal volume of DMSO as Blebbistatin treatments. For tricaine time point experiments, animals were left
657 in 0.5mg/mL tricaine in ASW for 3-50 hours.
658
659 **Immunostaining**
660 For antibody staining, all steps were carried out using an orbital shaker. Fixed animals were washed in
661 PBST for 3x5 minutes, then placed in blocking solution (PBST + 10% goat serum (Thermo Fisher,
662 16210072)) for one hour at room temperature. Animals were then placed in primary antibody in block
663 solution for two nights at 4ºC. Primary antibody was washed out with PBST, 6x20 minutes. Animals were
664 then blocked once again for one hour at room temperature, then incubated with secondary antibody
665 (1:800) (Thermo Fisher, A-11011) in blocking solution overnight at 4ºC. The next day, secondary antibody
666 was washed out using PBST, 6x20 minutes. Finally, animals were incubated in SiR-actin (1:1000) in
667 PBST (Cytoskeleton, CY-SC001) for 90 minutes at room temperature prior to mounting. All samples were
668 mounted on double cover slips using Prolong Glass Antifade Mountant (Thermo Fisher, P36980). If
669 animals were only stained with SiR-actin, they were placed in SiR-actin in PBST for 90 minutes at room
670 temperature, then mounted immediately. The custom *H. miamia* Tropomyosin antibody[80] (Rabbit IgG)
671 was used at 1µg/mL Where relevant, Hoechst (1:500) (Invitrogen, H3570) was used to counter-stain
672 nuclei.
673
674 **Generation of custom collagen IV antibody**
675 Rabbit polyclonal antibodies were custom-made by GenScript through their PolyExpress immunization
676 protocol, using a peptide sequence from *H. miamia* Collagen IV (CPPGAKGNDGEPGEKG). This peptide
677 was expressed in *E. coli* using the provided sequence and then used to immunize two rabbits. Two
678 antibodies were generated, purified, and validated in-house by Western Blot with the protein immunogen.
679
680 **Microscopy and image processing**

681 All images were collected using 10x/0.25x (dry), 20x/0.75x (dry), or 63x/1.40 (oil) fluorescent objectives
682 on a Leica DMI SP8 inverted confocal microscope, equipped with Leica Application Suite software.
683 Images were processed using Image J/FIJI software.
684
685 **Quantifications**
686 ***Length of epithelial basal protrusions***
687 To quantify the average length of basal protrusions in outer epidermal and pharyngeal epithelial cells,
688 images were taken of labeled cells in *EpiA:RFP* animals. The Measure function in FIJI was used to
689 quantify the length of each protrusion, tracing from the end of the protrusion to where it meets the body of
690 the cell. For each cell type (pharyngeal epithelium vs. outer epidermis), *n*=15 cells from n=5 animals (total
691 = 45 cells) was measured.
692
693 ***Percentage of closure in transverse amputations***
694 For quantification of wound closure in transverse cuts, images were taken of both the wound edge and
695 the open edge of each sample, using FIJI to measure the open area of each side. The percentage of
696 wound closure was determined by dividing the open area of the wound edge by the total open area, then
697 subtracting that from 1. For each time point and fragment (head vs. tail), measurements were collected
698 from *n*=8 animals.
699
700 ***Percentage of closure in sagittal amputations***
701 To quantify the percentage of wound closure after sagittal amputations, images of SiR-actin-stained
702 fragments were imported into FIJI. Because of mounting imperfections, only one side of each animal was
703 measured, choosing the side with the clearest signal for the most accurate quantification. 6-12 animals
704 were quantified per time point and condition. Within FIJI, the Measure function was used to quantify: 1)
705 the length of the pharynx and 2) the cumulative distance of connected tissue between the epidermis and
706 the pharyngeal epithelium. The percentage of wound closure was determined by dividing the closed
707 distance by the total pharynx length. For each time point, measurements were collected from *n*=12
708 animals.

709

710 ***Bridge length***

711 To quantify the length of heterotypic bridges, images of SiR-actin-stained fragments were taken at each
712 time point, then imported into FIJI for analysis. Using the Measure function, bridges were quantified by
713 drawing a line along the membrane extensions protruding between cell types. Cell bodies were not
714 included in this measurement. Because of the technical challenge of robustly identifying where one
715 protrusion met the other, the combined bridge length was reported instead of individual cell contributions.
716 For each time point, measurements were collected from *n*=30-40 animals.

717

718 ***Morphological descriptions***

719 To report the morphological characteristics of healing fragments, images of SiR-actin-stained fragments
720 were taken at each time point. For bridge formation, animals were binned into four categories: none (no
721 visible polarization of the epithelial layers and no protrusions), polarization (visible polarization of cell
722 membranes towards the wound edge), protrusions (at least one membrane extension <15um in length),
723 or bridges (at least one connected heterotypic bridge). For protrusion origin, animals were assessed for
724 visible protrusions coming from only the outer epidermis, only the pharyngeal epithelium, both, or neither.
725 Rounding was assessed by looking at the shape of the animal, binning animals into either open (no
726 visible rounding), rounding (partway through the rounding process), or closed (where the outer edges of
727 the fragments have met, re-forming a cylindrical body plan). The values plotted for each morphological
728 trait were the representative percentage of total fragments, ranging from *n*=10-45 animals (exact values
729 are reported in accompanying figure legends).

730

731 **Graphing and statistical analyses**

732 All graphs were generated using GraphPad PRISM. Data with two or more factors were analyzed using
733 two-way ANOVA with Dunnett's multiple comparisons test. Data comparing changes in one condition over
734 different time points were analyzed by one-way ANOVA with Dunnett's multiple comparisons test. A two-
735 tailed unpaired *t*-test with Welch's correction was used to compare data between two independent
736 groups. All statistical tests are stated in figure legends. *P* values were obtained using GraphPad PRISM

737 and used to determine the level of varying significance between experimental groups; groups were

738 considered different when $P<0.05$.

ACKNOWLEDGEMENTS

APK is a Fellow of the Jane Coffin Childs Memorial Fund for Medical Research. This project was supported by grants from the National Institute of General Medical Sciences of the NIH to MS: R35GM128817 and R35GM153252. Thanks to members of the Srivastava Lab for feedback on the manuscript.

AUTHOR CONTRIBUTIONS

A.P.K conceived the project, performed experiments, quantified and analyzed data, and wrote the manuscript under the supervision of M.S. Both authors discussed the results and edited the manuscript.

COMPETING INTERESTS

None declared.

751 **FIGURES AND FIGURE LEGENDS**

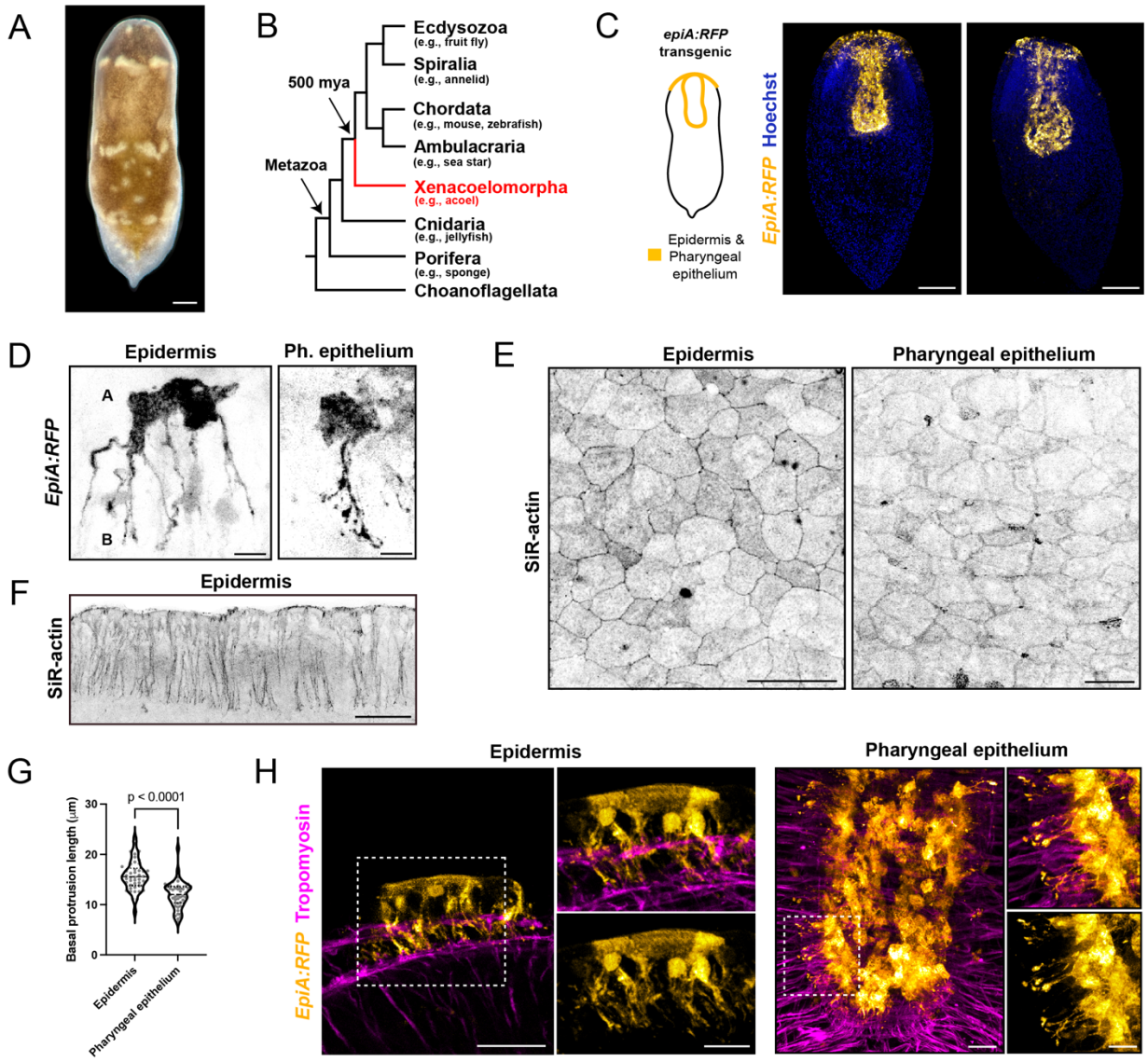

752

753 **Figure 1. *Hofstenia miamia* have two distinct, atypical epithelial tissues**

754 (A) A juvenile *Hofstenia miamia.* (B) A simplified phylogenetic tree showing the position of *Hofstenia*

755 *miamia* (red, Xenoacoelomorpha) relative to other clades. mya = million years ago. (C) *EpiA:RFP*

756 transgenic worms, fluorescently labeling the outer epidermis and the pharyngeal epithelium in a mosaic

757 manner. (D) Morphology of individual epidermal and pharyngeal (Ph.) epithelial cells, visualized by

758 *EpiA:RFP* transgenic labeling. A: apical, B: basal. (E-F) SiR-actin staining showing the apical organization

759 of *H. miamia* epithelial tissues, particularly the polygonal shape of each cell and the presence of actin at

760 cell-cell junctions (E) and the presence of actin within epidermal basal protrusions (F). (G) Quantification

761 of basal protrusions within epidermal and pharyngeal epithelial cells. Data represent n=45 cells per cell
762 type, pooled from 15 worms. Comparison by unpaired *t*-test. (H) Confocal images showing the proximity
763 of muscle (visualized through immunofluorescence staining for tropomyosin) to both epithelial layers
764 (visualized with EpiA:RFP transgenic labeling). Scale bars: 50 μm (A), 100 μm (C), 5μm (D), 20 μm (E,
765 H), 25μm (F), 10 μm (H, zoomed-in box).

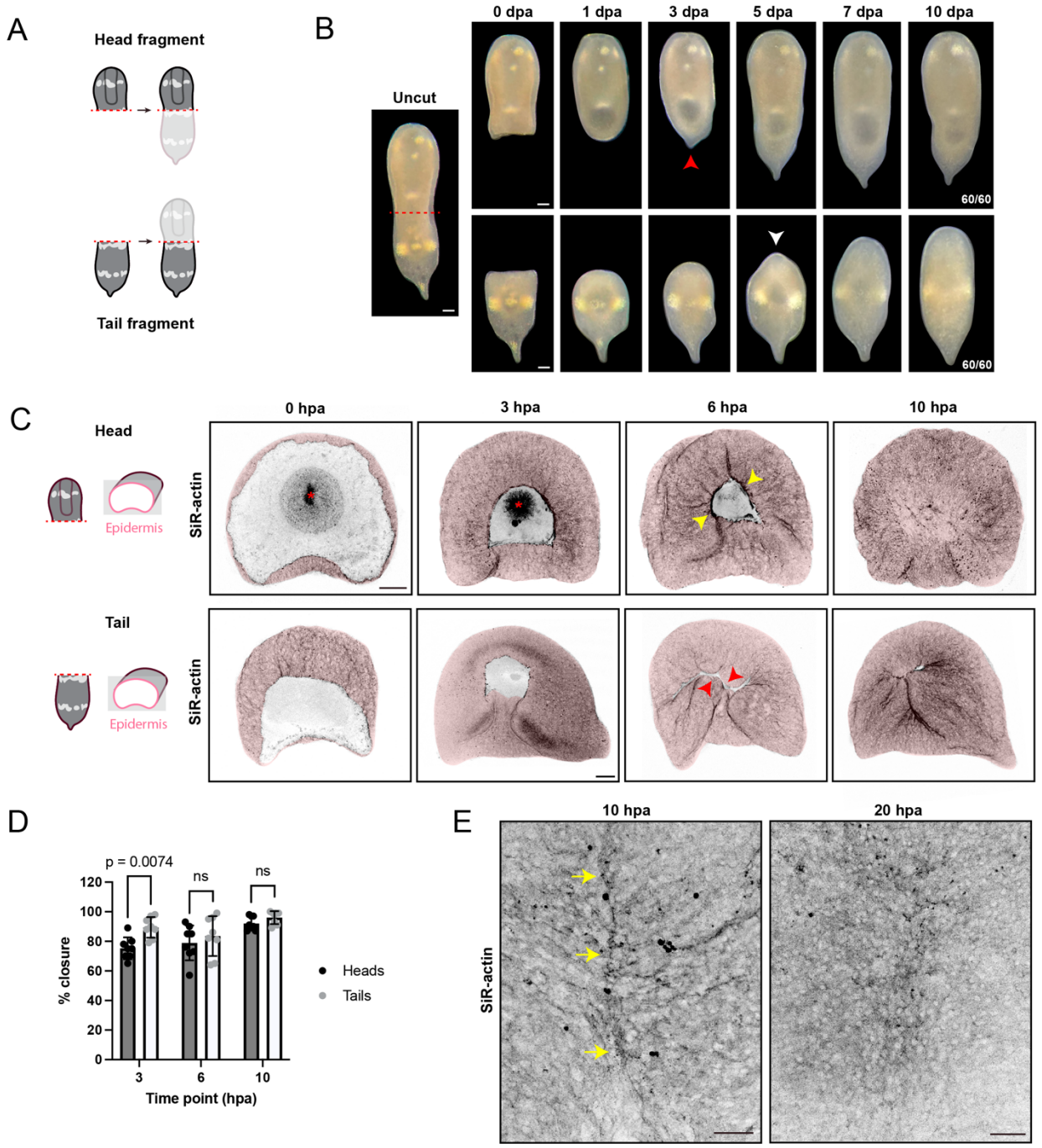

Figure 2. Transverse amputations close through gradual constriction of the epidermis across the wound edge.

(A-B) Schematic (A) and representative brightfield time course (B) showing regeneration of *H. miamia* following transverse amputation. Red arrowhead indicates the formation of a pointed tail, white arrowhead indicates a visible blastema. (C) Representative images of wound closure following transverse

772 amputation between 0-10 hours post-amputation. Red asterisk indicates the base of the pharynx, visible
773 in open wounds. The outer epidermis is pseudocolored in pink for clarity. (D) Quantification of wound
774 closure following transverse amputation, comparing between head and tail fragments from 3-10 hours
775 post-amputation. Data represent 8 worms per time point, and comparisons were performed by 2-way
776 ANOVA with Šidák's multiple comparisons test; ns=not significant. (E) High-magnification images
777 showing continued dynamics of re-epithelialization following initial closure; yellow arrows indicate a visible
778 seam where the tissue layers were brought together, but seams are no longer visible by 10 hours later.
779 hpa = hours post-amputation. Scale bars: 50μm (B), 100 μm (C), 25 μm (E).

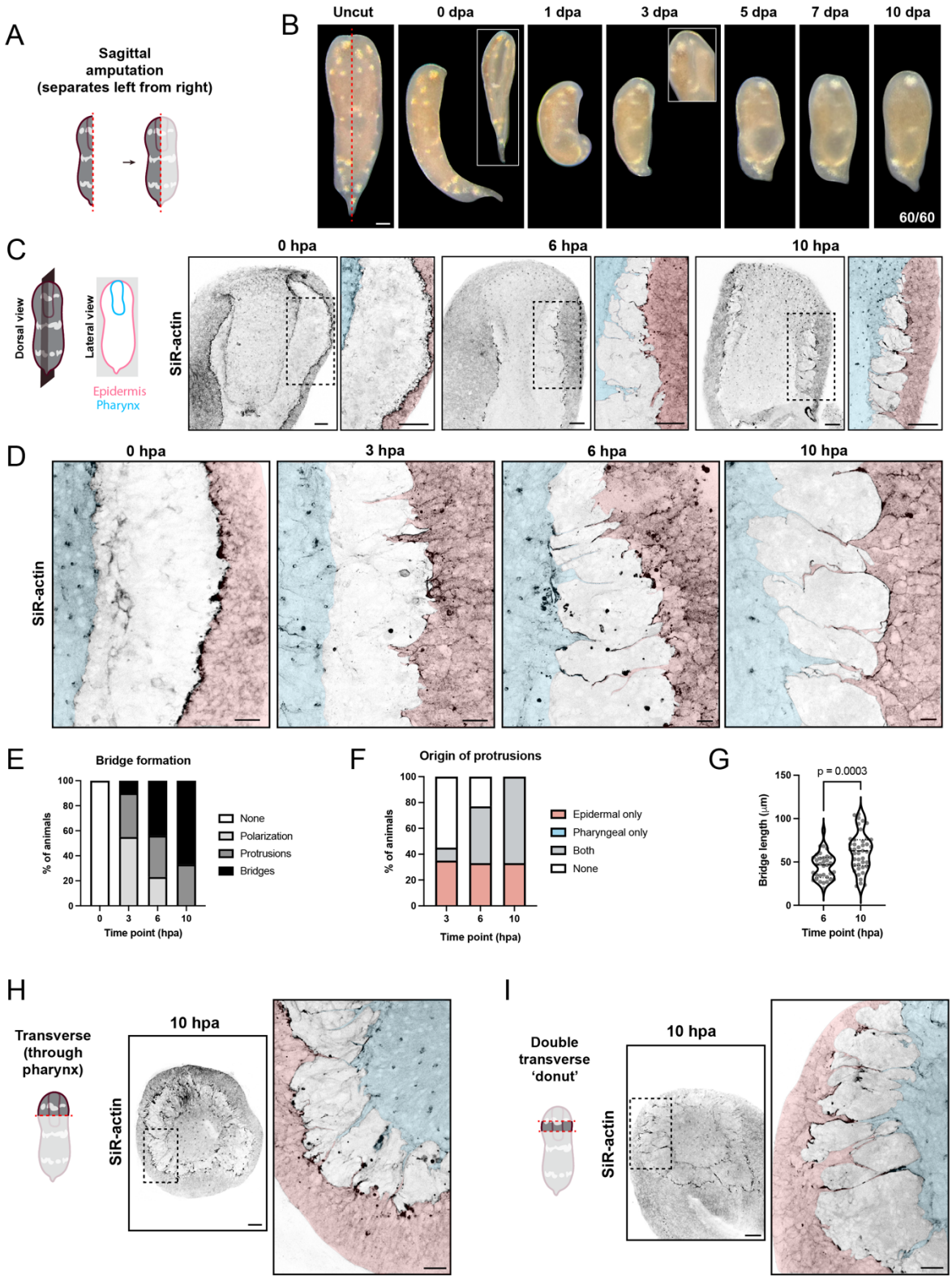

Figure 3. Injuries that damage both epithelial tissues form long, heterotypic protrusions connecting the epithelial layers across the wound edge

783 (A-B) Schematic (A) and representative brightfield time course (B) showing regeneration of *H. miamia*
784 following sagittal amputation. (C) Representative images of wound closure following sagittal amputation
785 between 0-10 hours post-amputation. (D) High-magnification images showing polarization, protrusion,
786 and formation of heterotypic bridges during the first 10 hours of wound closure. (E-G) Quantifications of
787 heterotypic bridge formation (E), origin of protrusions (F), and combined bridge length (G) over the first 10
788 hpa. Data represent 8 worms per condition and time point (E-F) and 30-40 bridges per time point (G);
789 comparison by unpaired *t*-test. (H-I) Representative images demonstrating the presence of heterotypic
790 bridges in single (H) and double (I) transverse amputations through the pharynx. In all high-magnification
791 images, the outer epidermis is pseudocolored in pink and the pharyngeal epithelium is pseudocolored in
792 blue for clarity. Scale bars: 50μm (B-C, H-I), 10 μm (C, zoomed-in box), 5 μm (D), 20 μm (H-I, zoomed-in
793 box).

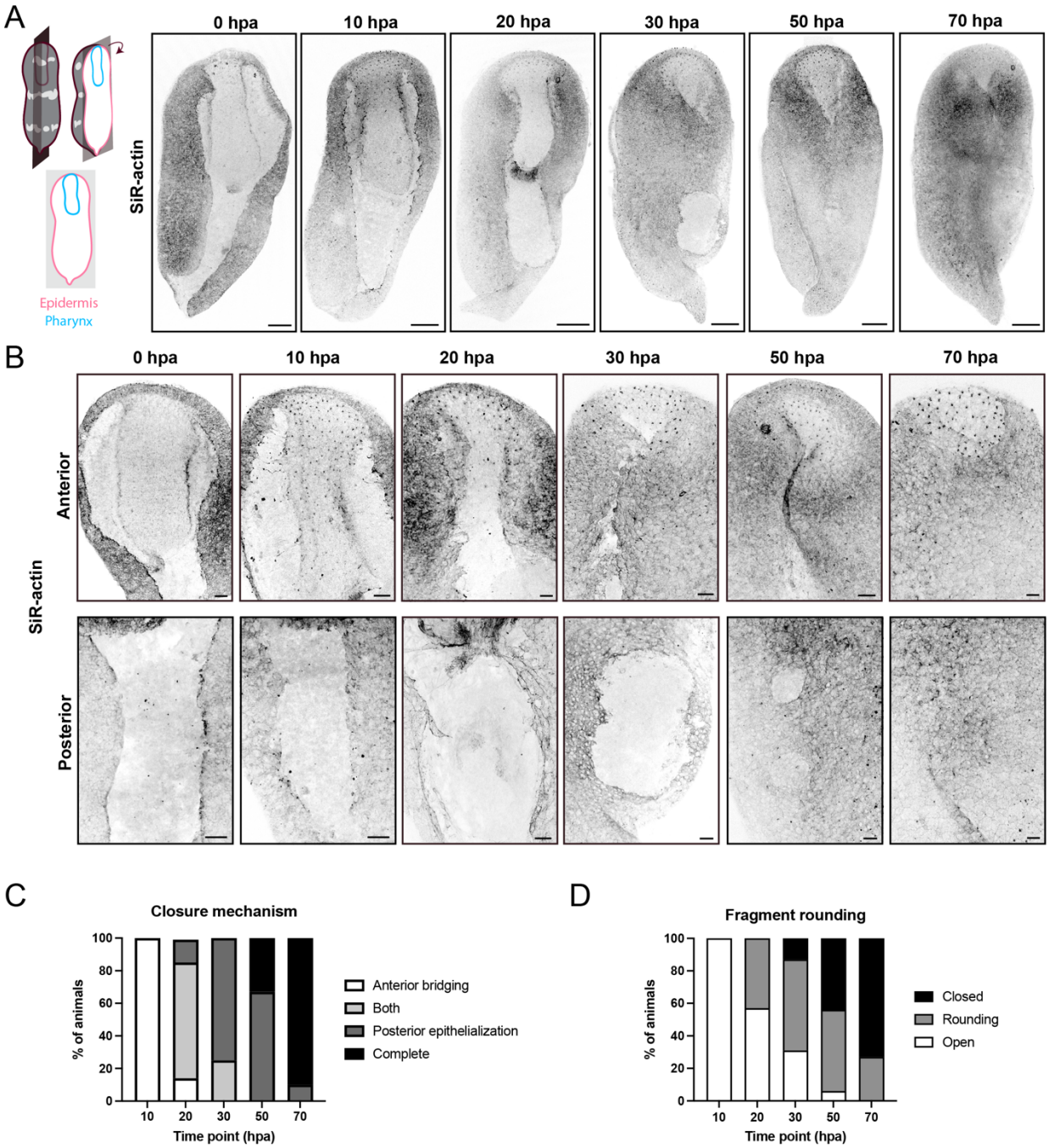

Figure 4. Sagittal wounds heal through a two-step process, combining epithelialization with whole-body rounding to restore the fragment's original morphology.

(A) Schematic and time course showing epithelial tissue dynamics in sagittal wound closure during the first 70 hours post-amputation (hpa), using SiR-actin labeling. (B) Higher-magnification images demonstrating the overlapping mechanisms of epithelialization in the anterior and posterior parts of the

800 fragment. Anterior tissues form heterotypic protrusions described in Figure 3, and the posterior wound
801 edges gradually close through homotypic re-epithelialization. (C-D) Quantifications of closure
802 mechanisms (C) and fragment rounding (D). Data represent n=12 animals per time point. hpa = hours
803 post-amputation. Scale bars: 100 μm (A), 20 μm (B).

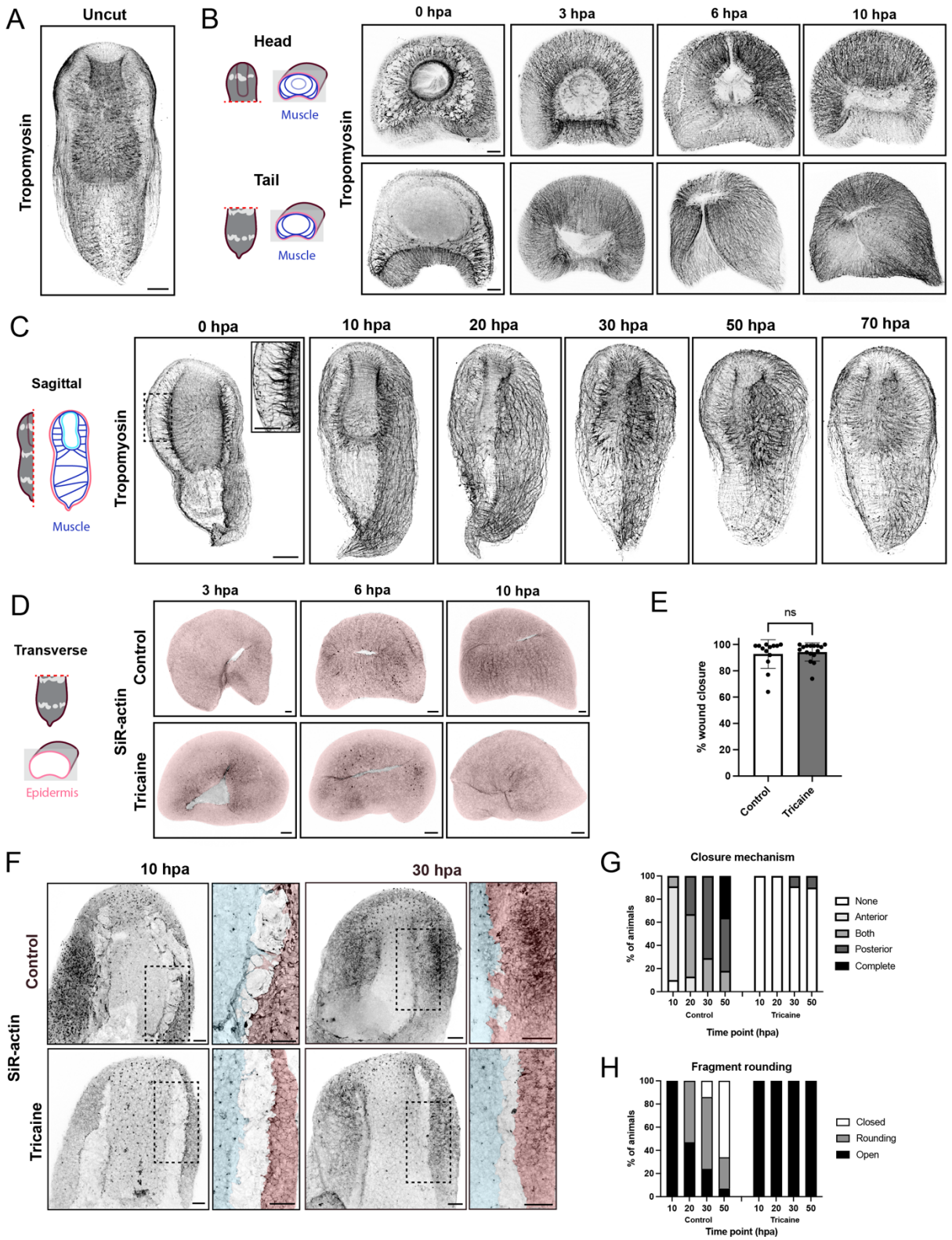

Figure 5. Muscle contraction is dispensable for traditional transverse amputations but required for the formation of heterotypic bridges during sagittal wound closure.

807 (A-C) Images showing the organization of muscle in uncut worms (A), transverse wound closure (B), and
808 sagittal wound closure (C), visualized by immunofluorescence staining for tropomyosin. (D-E)
809 Representative images (D) and quantification (E) of wound closure in control and tricaine-treated animals
810 after transverse amputation, labeled with SiR-actin. (F) Representative images of wound closure in
811 control and tricaine-treated animals after sagittal amputation, labeled with SiR-actin.
812 In D and F, the outer epidermis is pseudocolored in pink and the pharyngeal epithelium is pseudocolored
813 in blue for clarity. (G-H) Quantification of closure mechanism (G) and fragment rounding (H) in control and
814 tricaine-treated animals after sagittal amputation. Data represent n=12 animals per condition, per time
815 point; quantification in (E) by unpaired *t*-test. ns=not significant, hpa = hours post amputation. Scale bars:
816 100 μm (A,C), 50 μm (B,D,F).

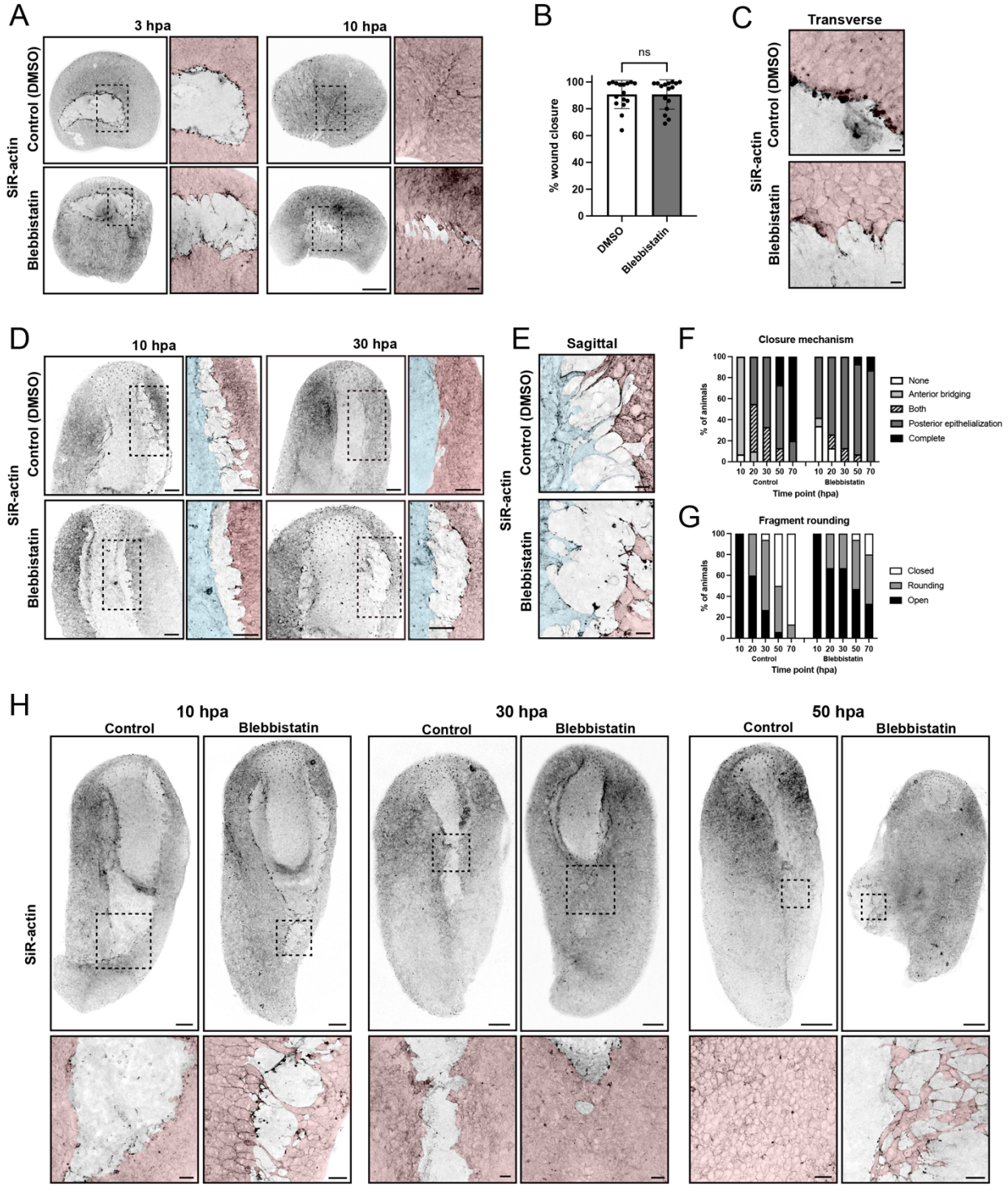

Figure 6. Actomyosin contractility is differentially utilized across wound closure mechanisms. (A-B) Representative images (A) and quantification (B) of wound closure in control and blebbistatin-treated animals after transverse amputation, labeled with SiR-actin. (C) High-magnification images

821 showing the difference between control and blebbistatin-treated wound edges in transverse amputations.
822 (D) Representative images of wound closure in control and blebbistatin-treated animals after sagittal
823 amputation. (E) High-magnification images showing heterotypic bridges in control animals and the lack
824 thereof in blebbistatin-treated animals. (F-G) Quantification of closure mechanism (F) and fragment
825 rounding (G) in control and blebbistatin-treated animals after sagittal amputation. (H) In high-
826 magnification images, the outer epidermis is pseudocolored in pink and the pharyngeal epithelium is
827 pseudocolored in blue for clarity. Data represent n=12-16 animals per condition, per time point;
828 comparison in (B) by unpaired *t*-test. ns=not significant, hpa = hours post amputation. Scale bars: 50 μm
829 (A,D), 10 μm (C,E), 100 μm (H), 20 μm (H, zoomed-in box).

SUPPLEMENTARY FIGURES AND TABLES

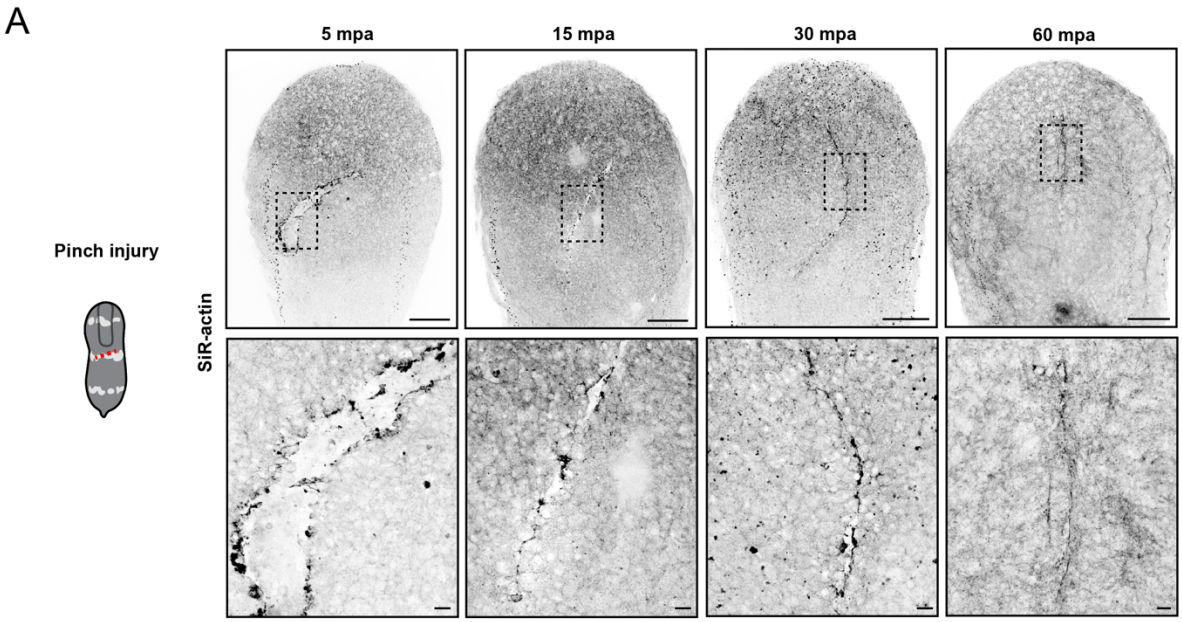

Supplementary Figure 1. Pinch wounds heal rapidly, utilizing cell protrusions to bring the wound edges together.

(A) Schematic and representative images showing wound closure following an epidermal pinch injury, labeled with SiR-actin. Scale bars: 100 μm (A, top row), 10 μm (A, zoomed-in box). mpa = minutes post amputation.

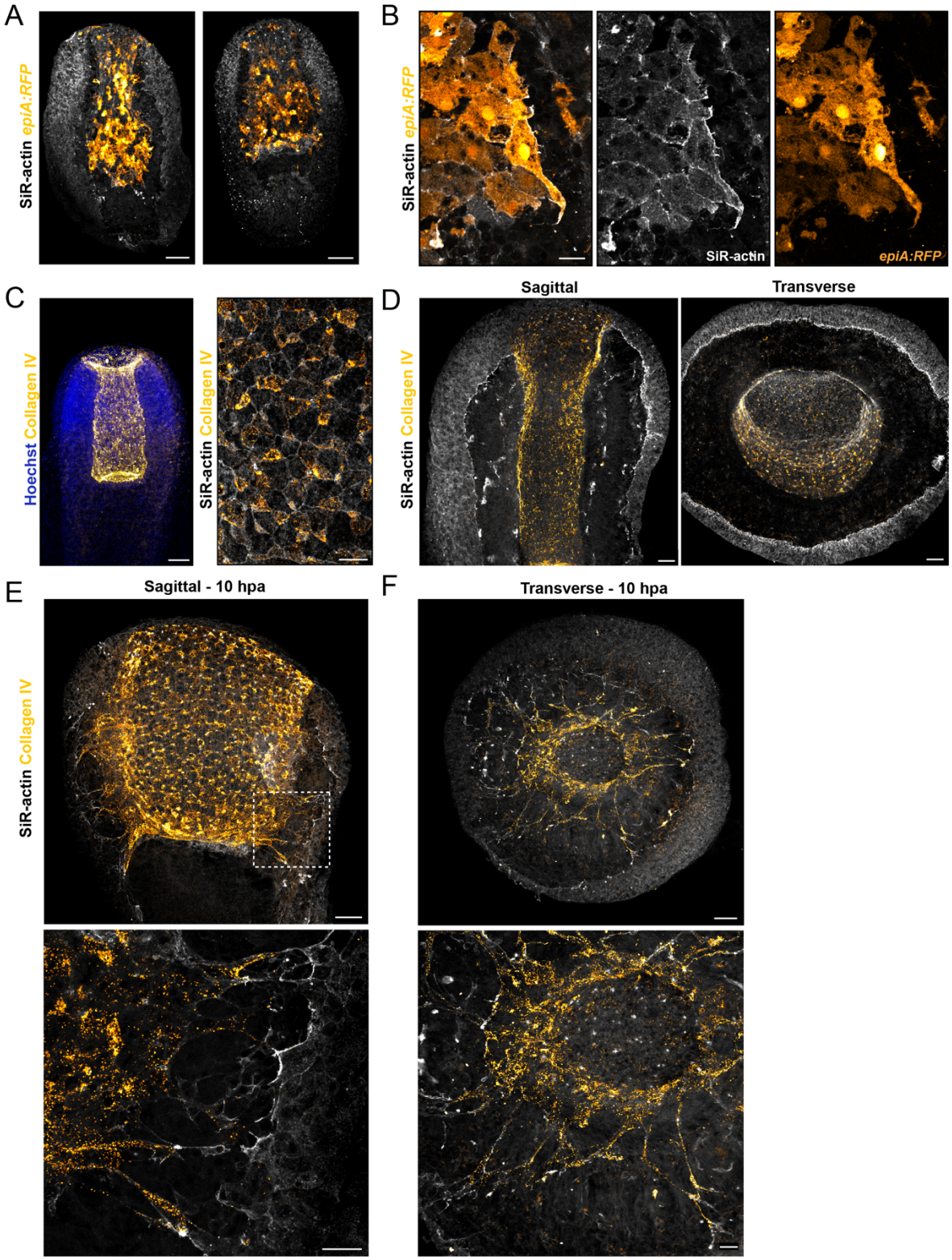

Supplementary Figure 2. Collagen IV is visible underneath pharyngeal, but not epidermal, protrusions during wound closure.

840 (A-B) *EpiA:RFP* transgenic animals cut in the sagittal plane have mosaic expression of RFP in both the
841 epidermis and the pharyngeal epithelium (A), and these cells are part of the SiR-actin-labeled population
842 that is forming protrusions during wound closure (B). (C-F) Immunofluorescence staining using a custom
843 Collagen IV antibody (see Methods) showing localization underneath the pharyngeal epithelium in uncut
844 (C) and 10 hours post-amputation (hpa) (D-F) fragments. Scale bars: 50μm (A, C (left), D, E-F (top)),
845 10μm (B), 20μm (C (right), E-F (bottom)).

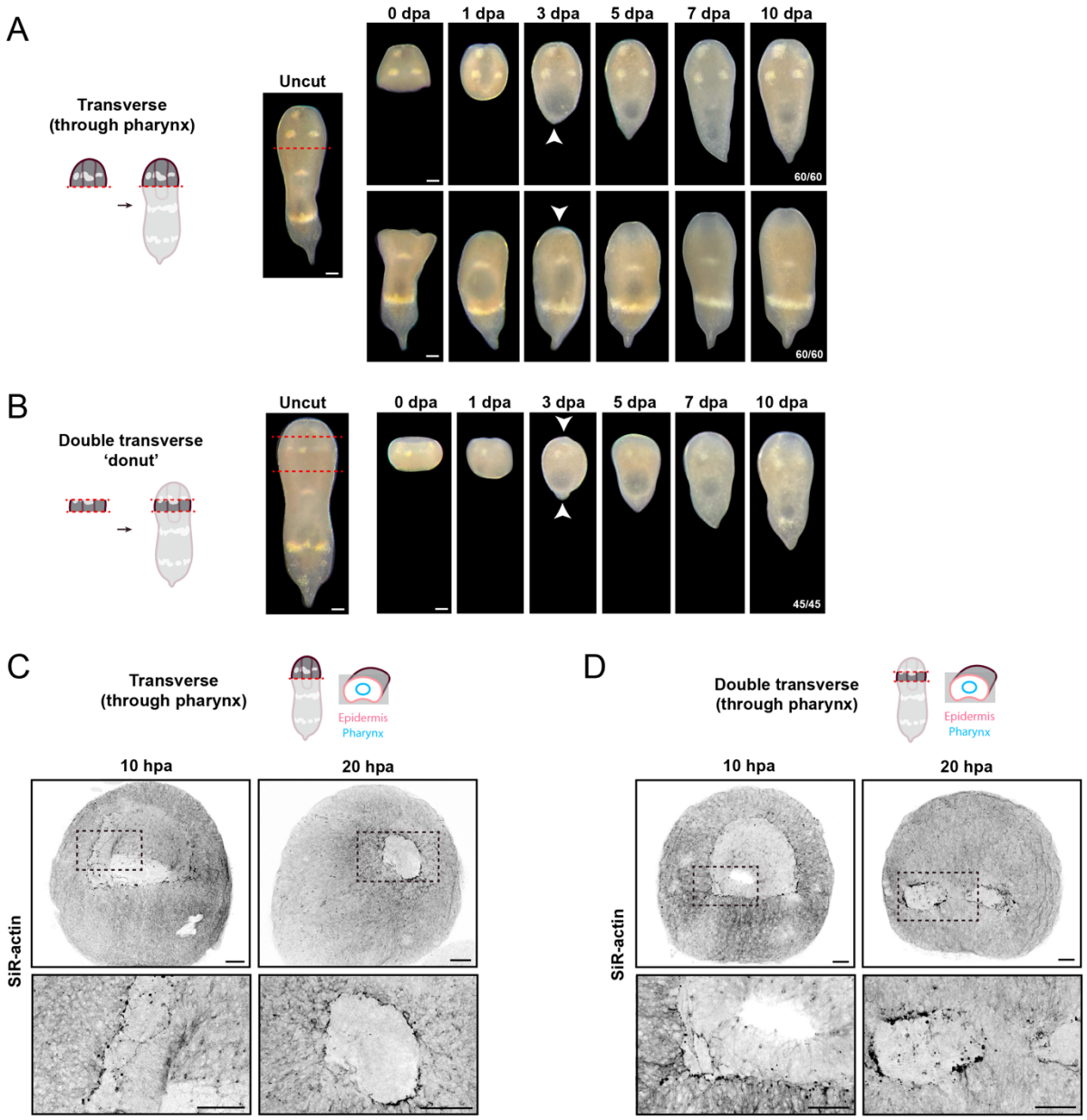

Supplementary Figure 3. Transverse amputations that injure the pharyngeal epithelium heal through a similar two-step mechanism.

(A-B) Schematic and representative brightfield time course showing regeneration of *H. miamia* following single (A) and double (B) transverse amputation. (C-D) Representative images showing wound closure following single (C) and double (D) transverse amputation, labeled with SiR-actin. Scale bars: 100µm (A-B), 50µm (C-D).

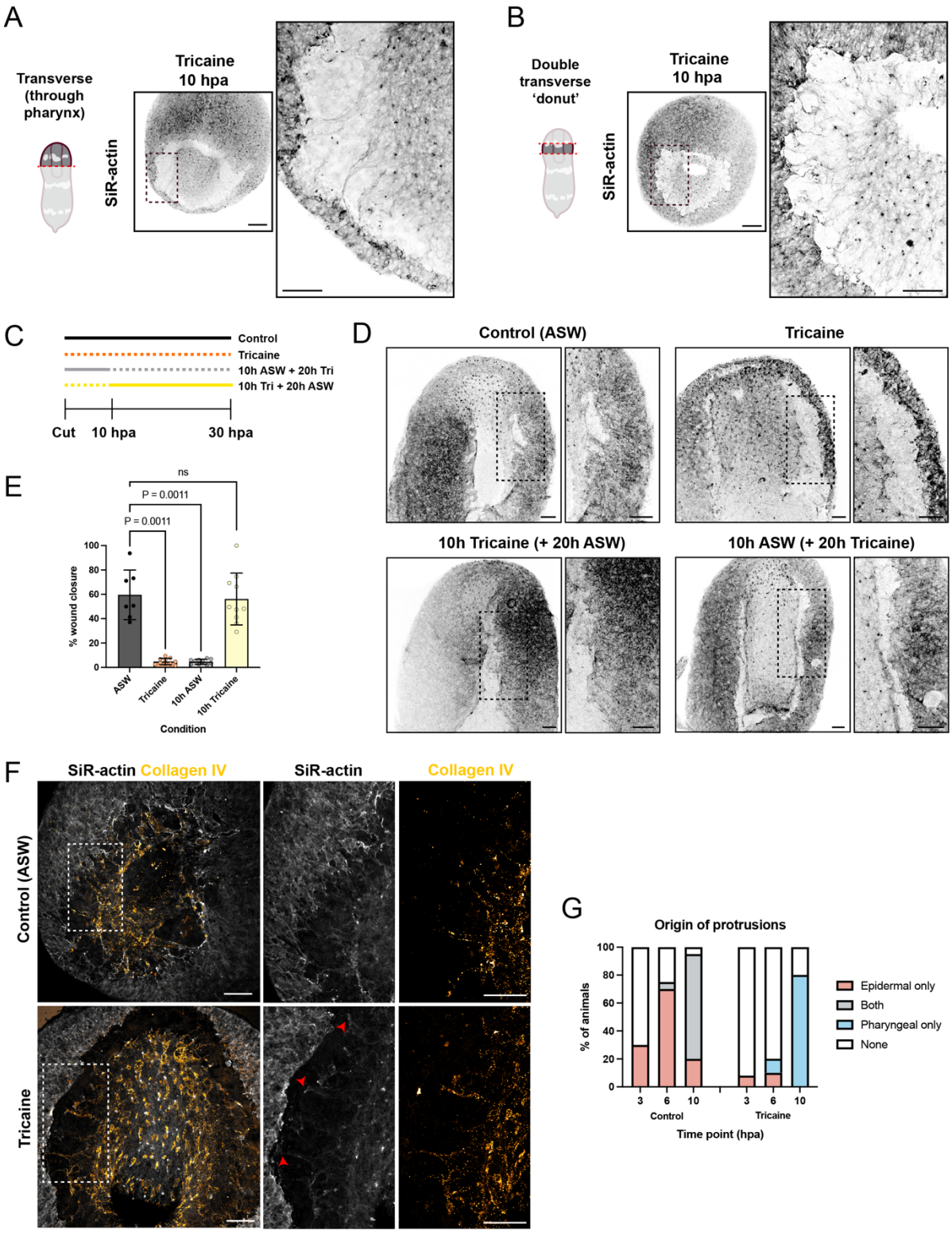

853

854 **Supplementary Figure 4. Muscle contraction is required for epidermal protrusions during**

855 **heterotypic bridge formation.**

856 (A-B) Representative images showing pharyngeal protrusions after single (A) or double (B) transverse
857 amputation in tricaine-treated conditions. (C) Schematic of tricaine timing experiment. (D) Representative
858 images showing wound closure in control, tricaine, 10h tricaine (+ 20h ASW), or 10h ASW (+ 20h tricaine)
859 conditions. (E) Quantification of wound closure across tricaine conditions. Data represent n=8 worms per
860 condition and show mean ± s.e.m. Comparisons by one-way ANOVA with Dunnett's multiple comparisons
861 test; ns=not significant. (F) Representative images showing Collagen IV localization underneath
862 pharyngeal extensions following transverse amputation in control and tricaine-treated conditions. (G)
863 Quantification of protrusion origin in control and tricaine-treated animals. Data represent n=7-10 animals
864 per condition, per time point. Scale bars: 100μm (A,B), 50μm (A,B (zoomed-in boxes), D,F).

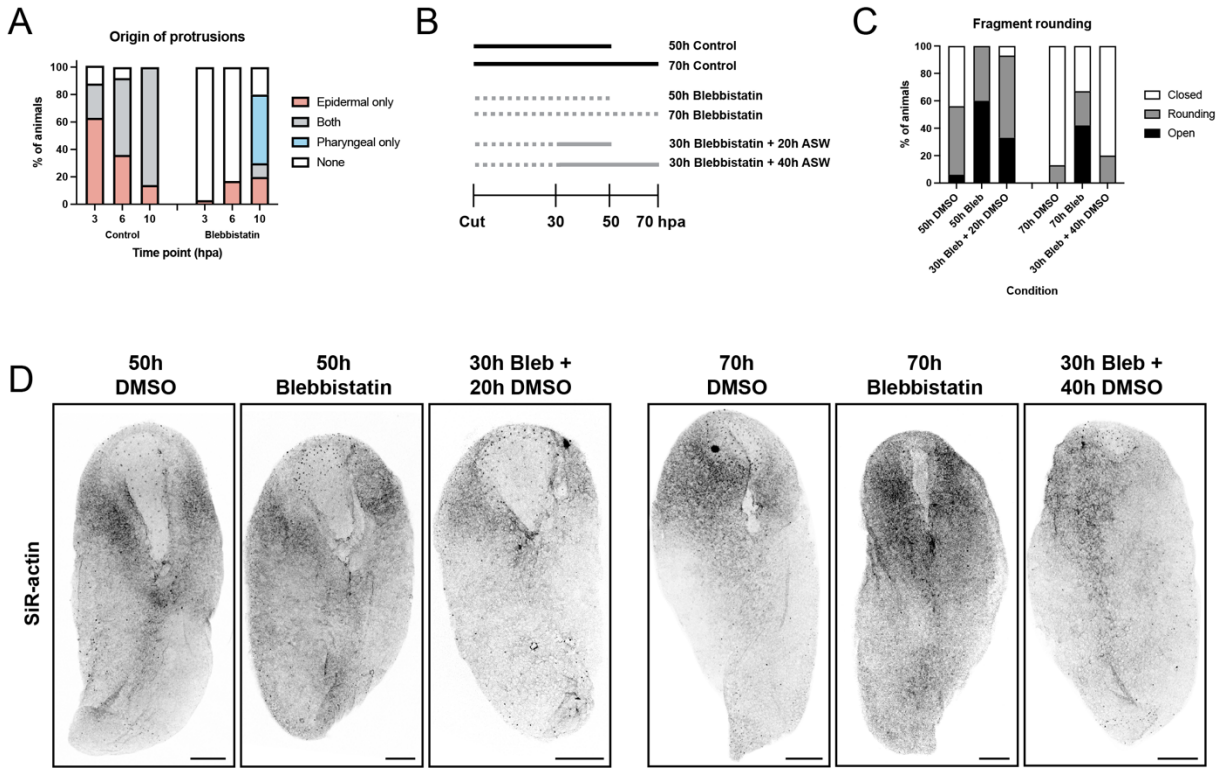

Supplementary Figure 5. Blebbistatin treatment is reversible.

(A) Quantification of protrusion origin in control and blebbistatin-treated animals. (B) Schematic of blebbistatin wash-out experiment. (C-D) Quantification (C) and representative images (D) of fragment rounding following control and blebbistatin treatments. Data represent n=8 animals per condition, per time point. Scale bars: 100μm (D).

871 **Supplementary Video 1. Tricaine slows muscle contraction in *H. miamia*.**

872 Animals are anesthetized in 1mg/mL tricaine in ASW.